

THE EFFECTS OF THE HORIZONTAL COMPONENT OF THE  
EARTH STRESS FIELD IN GEOLOGICAL STRUCTURES

by

Zvi Grinshpan

---

A Thesis Submitted to the Faculty of the  
DEPARTMENT OF GEOSCIENCES  
In Partial Fulfillment of the Requirements  
For the Degree of  
MASTER OF SCIENCE  
In the Graduate College  
THE UNIVERSITY OF ARIZONA

1 9 7 6

STATEMENT BY AUTHOR

This thesis has been submitted in partial fulfillment of requirements for an advanced degree at The University of Arizona and is deposited in the University Library to be made available to borrowers under rules of the Library.

Brief quotations from this thesis are allowable without special permission, provided that accurate acknowledgment of source is made. Requests for permission for extended quotation from or reproduction of this manuscript in whole or in part may be granted by the head of the major department or the Dean of the Graduate College when in his judgment the proposed use of the material is in the interests of scholarship. In all other instances, however, permission must be obtained from the author.

SIGNED: Zvi Gritshpan

APPROVAL BY THESIS DIRECTOR

This thesis has been approved on the date shown below:

John R. Sturgul  
JOHN R. STURGUL  
Associate Professor of Geosciences

3 Jun 1976  
Date

## ACKNOWLEDGEMENTS

My special thanks are given to my thesis director, Dr. John R. Sturgul, for his expert guidance and moral encouragement during the completion of this thesis and to the members of my committee, Drs. Peter Coney and Paul E. Damon, for their constructive criticism of the thesis. I also wish to thank Professor A. E. Scheidegger of Zurich, Switzerland, for the field data that he furnished and for the picture of the Hochkönig massif.

I am grateful to the management of Cyprus Bagdad Copper Company for giving me some time off from the hectic schedule to rewrite the thesis. Special thanks are due to the mine superintendent, Mr. R. J. Bonnis, and the chief geologist, Mr. P. K. Medhi.

Very special thanks are due to a great lady, my wife Rachel, who was with me through the ups and downs but never gave up. Her words of encouragement were an inspiration to me. I also thank my father and mother, Baruch and Sonia Grinshpan, for the emphasis they put on higher education.

## TABLE OF CONTENTS

	Page
LIST OF ILLUSTRATIONS . . . . .	vi
LIST OF TABLES . . . . .	viii
ABSTRACT . . . . .	ix
1. INTRODUCTION . . . . .	1
2. STATEMENT OF PROBLEM . . . . .	3
3. PREVIOUS WORK . . . . .	6
Weathering . . . . .	6
Rheology of Rock in the Tectonosphere . . . . .	6
Stress Fields . . . . .	9
Geophysical Stress Field . . . . .	10
Stress Field in the Vicinity of a Rock Wall . . . . .	16
4. THE FINITE ELEMENT METHOD . . . . .	20
The Concept of Finite Elements . . . . .	20
Applications . . . . .	21
Theory . . . . .	24
5. GENERAL FORMULATION OF A FINITE ELEMENT MODEL . . . . .	31
Computer Programs . . . . .	34
6. APPLICATION OF FINITE ELEMENT MODELS TO THE STUDY OF STRESS FIELDS . . . . .	36
Finite Element Model of an Alpine Cross Section . . . . .	36
Formulation of the Model . . . . .	36
Discussion . . . . .	43
Finite Element Model of a Rock Wall . . . . .	50
Formulation of the Model . . . . .	50
Discussion . . . . .	52
7. CONCLUSIONS . . . . .	59
APPENDIX A: DEFINITION OF TERMS . . . . .	62
APPENDIX B: ALPINE SOLUTION . . . . .	64

TABLE OF CONTENTS--Continued

	Page
APPENDIX C: ROCK-WALL SOLUTION WITH EQUAL AND OPPOSITE STRESS APPLIED . . . . .	88
APPENDIX D: ROCK-WALL SOLUTION WITH NO HORIZONTAL STRESS . . . . .	114
REFERENCES . . . . .	141

## LIST OF ILLUSTRATIONS

Figure	Page
1. Stress state of materials described by Mohr circles . . . . .	11
2. Stress geometry in a protrusion . . . . .	15
3. A typical cross section of a slope deformed by spatically continuous mass creep . . . . .	17
4. A mesh used in the solution of the finite difference approximation for the biharmonic equation . . . . .	19
5. Boundary conditions . . . . .	33
6. Location map of Hochkönig massif and position of geological profile . . . . .	37
7. View of the terrain of the Höchkönig massif, looking north . . . . .	38
8. A north-south geological cross section of the Hochkönig massif . . . . .	40
9. Finite element model of Alpine cross section . . . . .	42
10. Maximum principal stress contours for Alpine cross section . . . . .	44
11. Vertical component of shear stress for Alpine cross section . . . . .	45
12. Mohr failure criteria . . . . .	46
13. Conjugate fracture system for Alpine cross section . . . . .	47
14. Stresses acting in opposite directions creating tensile stress for Alpine cross section . . . . .	49
15. Finite element model of rock wall . . . . .	51
16. Rock wall with horizontal stress equal and opposite . . . . .	53
17. Rock wall with horizontal stress calculated separately on each side . . . . .	53

LIST OF ILLUSTRATIONS--Continued

Figure		Page
18.	Maximum and minimum principal stresses, section A of rock-wall mesh, no horizontal stress applied . . . . .	55
19.	Maximum and minimum principal stresses, section A of rock-wall mesh, applied horizontal stress, equal and opposite . . . . .	56
20.	Maximum and minimum principal stresses, section A of rock-wall mesh, unequal horizontal stresses applied . . . . .	57
21.	Directions of maximum and minimum principal stresses for Alpine cross section. . . . .	60

## LIST OF TABLES

### Table

1.	Stress orientations in different layers of the Hochkönig massif . . . . .	13
2.	Applications of the finite element method to geotechnical engineering . . . . .	22
3.	Sequence of layers in the Hochkönig area . . . . .	39
4.	Values for physical properties of the Hochkönig layers . . . . .	41
5.	Values assigned for physical properties for the rock-wall model . . . . .	50

## ABSTRACT

The finite element method has been an important tool for solving engineering and related structural problems for two decades. It has only recently found an application in geosciences.

Finite element models were used to test the effect of the horizontal component of the earth stress field on and around a rock-wall structure. The stress field at the foot of the rock wall was found to be approximately 45 degrees from the vertical. Stress concentration as well as failure of material occurred at this point. The influence of the rock wall on the stress field away from a notch was found to be only slight.

The finite element method was also used as an indirect method to study the stresses in the interior of a mountain massif, the Hochkönig massif in the Austrian Alps. It was possible to obtain a correlation between in situ measurements and data obtained by the finite element method.

## CHAPTER I

### INTRODUCTION

A three-part study has been conducted to determine:

1. Stress and strain effects near a rock wall due to the earth's gravity field.
2. Influence of equal amounts of horizontal pressure applied from both sides of a modeled rock wall.
3. Stress-strain fields in a two-dimension cross section of the Hochkönig massif in the Austrian Alps.

The solutions were obtained by application of the finite element method to problems of plain strain.

The Institute of Geophysics of the Technical University has carried out in situ measurements of stresses by the doorstopper method (described in Appendix A) in the Mitterberg copper mine situated in the Paleozoic basement beneath a calcareous mountain massif, the Hochkönig massif, in Austria. It was found by Brückl and Scheidegger (1974) that the presently acting stresses are qualitatively in agreement with those that would be expected if the stresses originated solely because of overburden.

It is the object of this thesis to test further the above qualitative observation by making a finite element calculation of the gravitational stresses by constructing a suitable geomechanical model of the mountain massif. The actual elastic properties of the rocks were used

for the calculation of a finite element model whose outlines match the real profile of the mountain range. The result was a close correspondence between the calculated stress orientations and those determined in situ.

## CHAPTER 2

### STATEMENT OF PROBLEM

The previous consensus was that most weathering occurring on the surface of the earth is due to exogenic effects. For example, the cirques created in the Alps were particularly attributed to weakening of the rock structure by ice.

Voight (1966) pointed out that endogenic weathering may be responsible for some geomorphological forms observed today. This idea was adapted by Gerber and Scheidegger (1969), who postulated that the endogenic weathering process may be influenced by the particular structural form of the rock mass. In general, the higher the rock mass, the larger the stress underneath it; and it follows that stress on slopes increases downslope.

Scheidegger (1974) examined the morphological forms in the Hochkönig massif in the Austrian Alps and was able to infer the stress field that caused them by two separate means: (1) directly by in situ measurements in a mine and (2) indirectly by plotting the joint orientations on a Schmitt net and deducing the principal stresses that created them. The maximum principal stress is at a 45-degree angle with each of the joint sets, and the intermediate and minimum principal stresses are normal to the maximum principal stress.

The direct method is by far the more accurate for studying the present stress field of a rock mass. This method, although adequate

for measuring the maximum principal stress, has several restrictions. One is expense, which can become prohibitive when attempting to study many location points. Another is accessibility, which is no less important. Scheidegger (1974) found the direct method useful for in situ measurements of the maximum principal stress but not for measurements of the intermediate or minor stress.

The indirect method is useful for determining the stresses that created the observed joints. But the stresses measured by the indirect method are not necessarily those that are active at present. They may have been induced by past tectonic processes. Also, gravity-induced stresses are not necessarily indicated by indirect measurements.

One of the ways to circumvent the problem inherent in these techniques is a numerical study of a model that resembles the actual case found in nature. One such study of the tectonic stresses surrounding a rock wall was conducted by Sturgul (1967). His conclusions was that there is a stress concentration at the foot of the wall, if one considered only a uniform horizontal stress field. This conclusions was proved to be accurate by actual measurements. Yet this method does not provide for the study of stresses in the interior of a more complex structure, such as a mountain mass like the Hochkönig massif. Two points distinguish the massif problem from the rock wall problem: (1) the rugged relief and (2) a layer-cake stratigraphy in which each layer exhibits different elastic properties.

This thesis consists of two parts. The first will present computations for the stress field and displacements of the nodes for an Alpine model, a two-dimensional cross section of the Hochkönig massif.

After values for cohesive strength of each rock type were assigned and some failure criteria were established, the maximum and minimum principal stresses were used to infer locations of possible failure.

The second part will show the adequacy of the finite element method in obtaining the stress field due to the earth's gravity field around a rock wall, and it will examine the influence of horizontal stress on that wall.

## CHAPTER 3

### PREVIOUS WORK

#### Weathering

The difference between exogenic and endogenic weathering of a rock mass, as defined in Appendix A, is the difference between fluvial and atmospheric-induced weathering and stress-induced weathering. Gerber and Scheidegger (1969) have described how the two types of weathering are manifested in nature. The stress-induced features, whether induced by a tectonic stress field or a self-generated stress field under gravity, are characterized by fracture patterns, such as cleavage cracks and faults. Exogenic agents generate a drainage net characterized by geometric randomness.

A third type of weathering, described by Scheidegger (1973) as due to a combination of exogenic and endogenic agents, is in all probability responsible for shaping many of the structures in nature.

#### Rheology of Rock in the Tectonosphere

In the application of seismic waves to geophysical prospecting, Dobrin (1960) considers transverse and longitudinal waves moving through a perfectly elastic medium. Seismic waves can be introduced into the earth by controlled explosions whose energy is propagated through the earth as longitudinal (compressional) and transverse (shear) wave. The wavelength  $\lambda$ , velocity  $V$ , and frequency  $f$  of each of the wave forms are

related by the formula:

$$\lambda = \frac{V}{f} \quad (3-1)$$

Velocity is dependent on several elastic constants, including the density of the medium in which the wave is propagated.

The velocity of longitudinal and transverse waves are related to the elastic constant and density by

$$\begin{aligned} V_p &= \left( \frac{k + (4/3)\mu}{\rho} \right)^{1/2} = \left( \frac{E}{\rho} \left( 1 + \frac{2\nu^2}{1 - \nu - 2\nu^2} \right) \right)^{1/2} \\ &= \left( \frac{E}{\rho} \frac{1 - \nu}{(1 - 2\nu)(1 + \nu)} \right)^{1/2} \end{aligned} \quad (3-2)$$

and

$$V_s = \left( \frac{\mu}{\rho} \right)^{1/2} = \left( \frac{E}{\rho} \frac{1}{2(1 + \nu)} \right)^{1/2} \quad (3-3)$$

where

$V_p$  = velocity of longitudinal wave

$V_s$  = velocity of transverse wave

$k$  = bulk modulus

$\mu$  = shear modulus

$\rho$  = density

$E$  = Young's modulus

$\nu$  = Poisson's ratio.

This elastic behavior of isotropic solid materials, that is, how strain (deformation) is related to stress (loading), can often be described to a first approximation by linear relationship:

$$\sigma = \lambda \delta \epsilon + 2\mu \epsilon \quad (3-4)$$

where

$\sigma$  = stress

$\delta$  = nodal displacement in a body divided into elements, with nodes at their four corners

$\lambda$  = a Lamé constant;  $\lambda = k - 2\mu/3$ .

$c$  = strain.

For isotropic materials, Young's modulus and Poisson's ratio can be defined in terms of the Lamé constants by the following equations:

$$E = \frac{\mu(3\lambda + 2\mu)}{\lambda + \mu} \quad (3-5)$$

$$\nu = \frac{\lambda}{2(\lambda + \mu)} \quad (3-6)$$

Another equation representing the stress in a viscous fluid is:

$$\sigma = 2\eta c \quad (3-7)$$

where

$\eta$  = viscosity

$c$  = change in strain with time.

Scheidegger (1970a, 1970b, 1971) has studied the rheology of the tectonosphere in the short, intermediate, and long time ranges. These ranges refer to time periods defined as: short, up to 4 hours; intermediate, 4 hours to 1,500 years; and long, more than 1,500 years.

In studying the long time range, Scheidegger obtained data from the isostatic behavior of post-glacier uplift. The elastic model for post-glacial relaxation effects were found to be too simple and inappropriate. The viscous model came close to describing the post-glacial uplift only if an arbitrarily chosen value was used for viscosity  $\eta$ . This model was also inappropriate because it yields exponential relaxation

patterns that do not seem to fit the behavior of post-glacial uplift. Scheidegger (1970b) concluded that the only satisfactory way to describe the glacial rebound curve is given by some logarithmic relationship between stress rate and strain rate. One possible form of this relationship is expressed as

$$\sigma = 2\eta\dot{\epsilon} + \beta\dot{\epsilon}^2 \quad (3-8)$$

where  $\beta$  is a creep factor. This model seems to be one that does not contradict the uplift data. However, in any future study, it should be noted that the terms  $\eta$  and  $\beta$  are hard to estimate.

The data for rheology of the earth in the intermediate time range was obtained from seismology, tidal investigations, and observations of the Chandler wobble. Again, the linear equations that lead to exponential creep were not satisfactory, and it was found that the behavior of the earth in the intermediate range could best be expressed by the logarithmic relationship of equation (3-8). The same holds true in the short time range. Evidence for the short time range was obtained from seismic wave transmission and laboratory studies.

Scheidegger (1972) therefore concluded that the rheology of the earth in all time ranges can only be described accurately by logarithmic relationships but the elastic model of equation (3-4) holds true for small stresses.

### Stress Fields

For a study of the fracture data, it was found that the Mohr criteria were most satisfactory. Anderson (1951) discussed the Mohr failure criteria. He stated that in a triaxial stress state two conjugate glide

planes form when the yield stress is exceeded. These planes form an angle of  $<45$  degrees with the maximum stress direction, and the intermediate principal stress direction is contained in one of these planes.

The state of stress of the materials described by the Mohr circle in Figure 1 has a yield condition represented by the Coulomb equation,

$$\tau_0 = \sigma \tan \phi + C \quad (3-9)$$

where  $\tau_0$  = the cohesive shear strength

$\sigma$  = normal stress

$C$  = a constant indicative of the cohesion of the material

$\phi$  = angle of internal friction.

$\sigma \tan \phi$  is also called the coefficient of internal friction (Fig. 1).

The material fails when  $\tau_0$  and  $\sigma \tan \phi$  are exceeded. These conditions are fulfilled at any point of intersection of two straight lines tangent to the Mohr circles. The equation for these lines can be written as:

$$\tau = \tau_0 + \sigma \tan \phi \quad (3-10)$$

The state of stress corresponding to point P (Fig. 1) is reached on a pair of surfaces intersecting in the  $\phi$  direction, with normals inclined at an angle  $2\alpha$  to the maximum stress ( $\sigma_1$ ) direction.

### Geophysical Stress Field

The stress field in the Hochkönig massif, a portion of the Austrian Alps, was studied by Scheidegger (1974) in three ways:

1. From joint orientations in the Paleozoic basement of the massif.
2. From joint orientations in the calcareous superstructure.

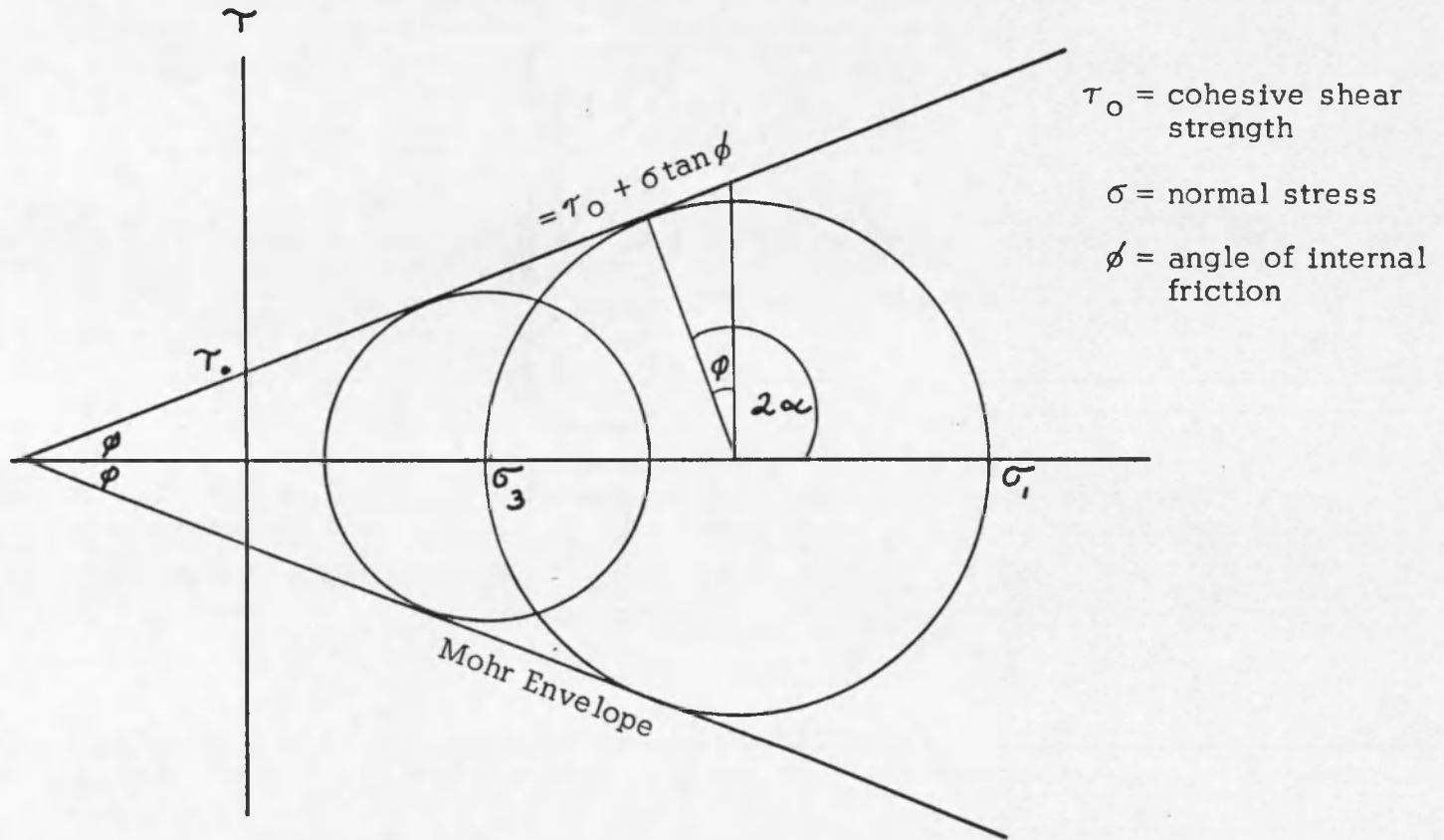


Figure 1. Stress state of materials described by Mohr circles

3. From in situ stress measurements taken by the doorstopper method in the Mitterberg copper mine situated in the Paleozoic basement of the massif.

Analysis of the first two parameters was done by field mapping joints in the rocks. The orientation of the joints were recorded by strike and dip. Measurements were made using a standard field geological compass. The joint parameters were plotted as poles (points) to the joint surfaces on an equal-area projection of the lower half of a unit sphere, and equidensity lines were drawn for the pole concentration. If two maxima were obtained in the equidensity diagrams these were regarded as conjugate Mohr fracture surfaces in a triaxial stress system. The maximum principal stress direction is inclined at an angle  $<45$  degrees toward the fracture surface and the intermediate principal stress direction is, of course, perpendicular to this direction. In the three-dimensional case, there would be two possible planes that could be drawn perpendicular to this direction, but by observing the type of failure and using Anderson's (1951) theory, the plane containing the intermediate principal stress is inferred. Thus, the three principal stress directions were inferred. The in.situ analyses were performed in a copper mine located in the Paleozoic graywackes. Three holes were drilled and the principal stresses were determined by the doorstopper method described by Brückl and Scheidegger (1974) (Appendix A).

Some of the conclusions reached in this particular study were:

1. The joint system in the Paleozoic graywackes are a result of a stress system that is different from the others active in the Alps.

2. The joint system of the Triassic limestone superstructure corresponds with the north-south thrust fault that is thought to have created the Alps.
3. The in situ stress measurements are entirely in conformity with the gravity effect of the summit of the Hochkönig; furthermore, it was found that the stress system is also in conformity with the makeup of the area and its topography.

A summary of the stress orientations in the different layers of the massif is given in Table 1

Table 1. Stress orientations in different layers of the Hochkönig massif

Locality	Stress Orientation <sup>a</sup>		
	$\sigma_1$	$\sigma_2$	$\sigma_3$
Graywackes	S 62° W 33°	N 50° E 59°	S 32° E 06°
Limestone superstructure	N 24° E 10°	S 00° W 78°	N 66° W 05°
Mannlwand	N 06° W 20°	S 51° E 63°	S 78° W 17°
In situ	S 23° E 70°	?	?

a.  $\sigma_1$ ,  $\sigma_2$ , and  $\sigma_3$  represent the maximum, intermediate, and minimum stresses, respectively.

Stress-induced weathering has its manifestation in the shaping of the Alps. Intuitively, it is understood that the higher a rock mass, the larger the concentration of stresses at the bottom. When the rock mass resembles a wall there exists a nonequilibrium stress situation where the overburden-induced stress is counteracted only by atmospheric

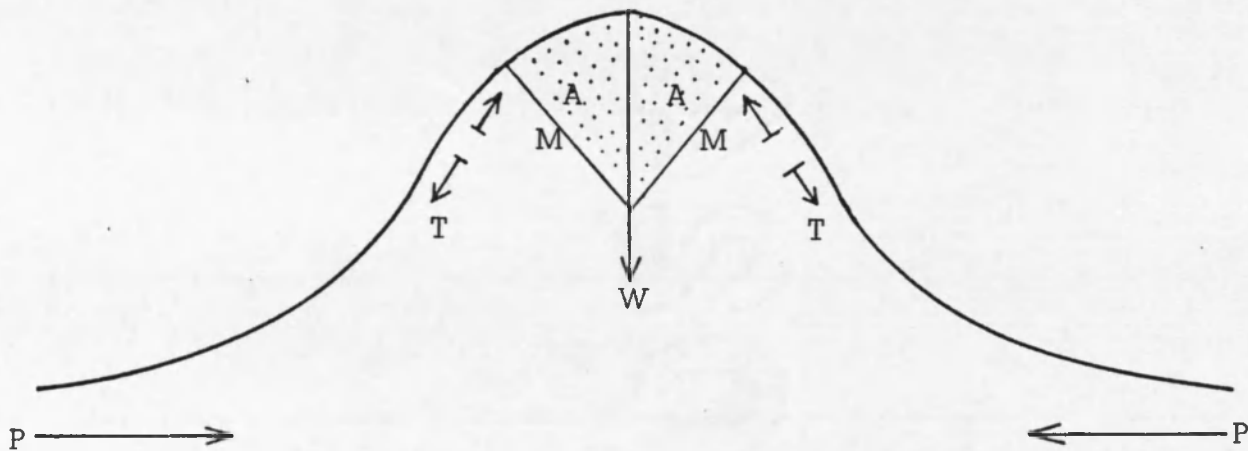
pressure. Therefore, the endogenic weathering at the Alps starts at the bottom as fractures and when completed on top leaves a straight wall (Gerber and Scheidegger, 1969).

When the stress of the overburden exceeds the tensile strength of the material underneath, the result can be plastic yielding. This was observed in the Alps where tower cliffs are standing behind a slope made of loose rock material broken from the cliff.

V-shaped gullies and valleys are another morphological phenomenon created by stresses attributed to the overburden. Gerber and Scheidegger (1969) have explained the V shape as a morphological expression of conjugate fracture surfaces induced by stress. These cleavages that form rock walls at 40 to 60 degrees to the horizontal were thought to have been formed by a tectonic stress field. In the following discussions it will be shown that conjugate fractures can also be indicative of stresses induced by the weight of the overburden.

Of utmost importance to some geomorphologists are the stresses active on mountain slopes and the resultant physical weathering. The effects of removal of overburden from an inclined surface has been studied by Sturgul and Grinshpan (1975) at the Grand Canyon. It was found that a possible mechanism for the folding of the Muav Limestone is elastic rebound caused by relief from the overburden pressure as material was eroded during the formation of the canyon.

A general schematic of the stress geometry in a protrusion was given by Gerber and Scheidegger (1969). Figure 2 shows tension cracks on the right flank as well as the maximum tension acting on the mountain slopes and the conjugate Mohr surfaces at a 45-degree angle to the



W = Maximum compression (weight)

T = Maximum tension

A = Breakout

M = Mohr surfaces

P Tectonic stress at infinity

Figure 2. Stress geometry in a protrusion.--From Gerber and Scheidegger (1969, Fig. 16).

maximum weight. It is known that the tensile strength of the rock material is very low; therefore, it is assumed that if failure occurs it will happen somewhere on the mountain slope.

A more comprehensive study of mass creep effect on Alpine slopes was conducted by Brückl and Scheidegger (1972). In their discussion they broke the slope down into its geomechanical components. In so doing they elaborated on work done by Ampferer (1939, 1940) and Stiny (1941).

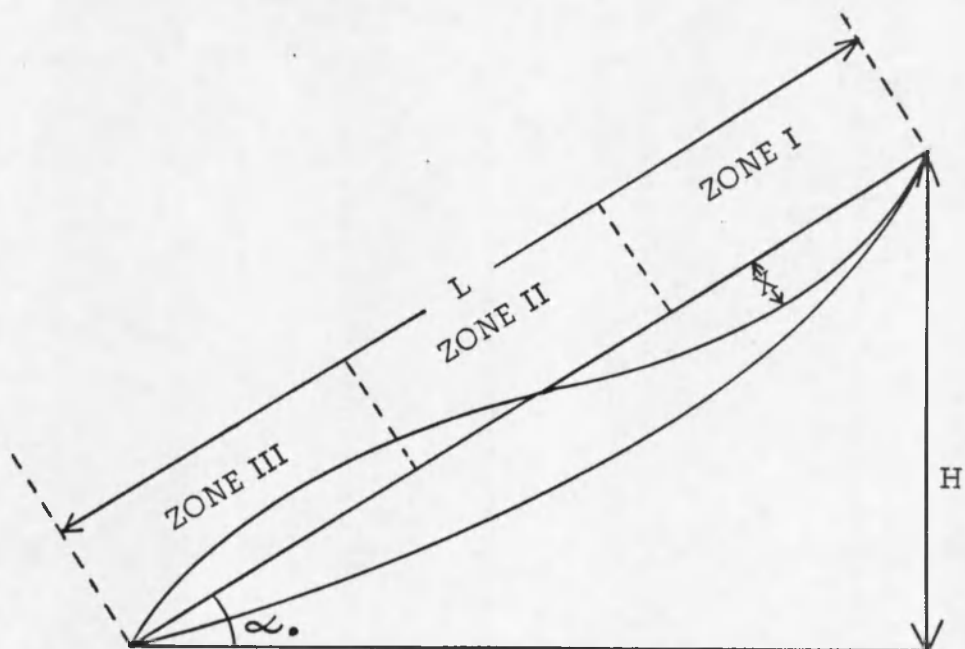
Figure 3 shows that tensional stresses operate in Zone I and shearing action is therefore active in this zone. Compressional stresses are active in Zone III. Shear stresses act parallel to the slope surface in Zone II.

#### Stress Field in the Vicinity of a Rock Wall

A rock wall in nature has been defined by Gerber and Scheidegger (1969) as a slope on which scree cannot accumulate. Such slopes are generally greater than 50 degrees and create a stress concentration at their bases. This stress concentration is considered to affect the weathering that always starts near the bottom

Sturgul and Scheidegger (1967) have numerically calculated the stress concentration around a vertical rock wall by using a finite difference approximation to obtain the stress field. The problem was set up as a plane stress problem.

To determine the state of stress in a homogeneous elastic body it is necessary to solve a system of equations given by Timoshenko and Goodier (1970) subject to given boundary conditions. Neglecting the



$\alpha_0$  = Slope inclination before creeping =  $27^\circ$

$L$  = Length of slope = 1650 m

$H$  = Height of slope = 750 m

$X$  = Displacement of creeping slope; creep velocity assumed = 100 cm/cm/yr

Figure 3. A typical cross section of a slope deformed by spatially continuous mass creep.--After Brückl and Scheidegger (1972)

body forces due to gravity, the basic equations are:

1. Equilibrium equations.

$$\frac{\partial \sigma_x}{\partial x} + \frac{\partial \tau_{xy}}{\partial y} = 0 \quad (3-11)$$

$$\frac{\partial \tau_{xy}}{\partial x} + \frac{\partial \sigma_y}{\partial y} = 0 \quad (3-12)$$

2. Compatibility equation.

$$\nabla^2(\sigma_x + \sigma_y) = 0 \quad (3-13)$$

The equilibrium equations imply the existence of a function  $\phi(x, y)$  such that

$$\sigma_x = \frac{\partial^2 \phi}{\partial y^2}; \quad \sigma_y = \frac{\partial^2 \phi}{\partial x^2}; \quad \tau_{xy} = \frac{\partial^2 \phi}{\partial x \partial y} \quad (3-14)$$

This function,  $\phi(x, y)$ , is also known as the Airy stress function. From the compatibility relations it is evident that the Airy stress function satisfies the fourth-order partial differential equation:

$$\nabla^2(\nabla^2 \phi) = \nabla^4 \phi = \frac{\partial^4 \phi}{\partial x^4} + 2 \frac{\partial^4 \phi}{\partial x^2 \partial y^2} + \frac{\partial^4 \phi}{\partial y^4} \quad (3-15)$$

This equation is called the biharmonic equation.

To use finite differences for the biharmonic equation, a system of nodes is selected as shown in Figure 4. If the nodes happen to fall outside the region under consideration, they are known as fictitious points and special care must be taken. The finite difference approximation solution for the biharmonic equation is

$$\begin{aligned} \nabla^4(\nabla^4 \phi_0) &= 20\phi_0 - 8(\phi_1 + \phi_2 + \phi_3 + \phi_4) \\ &\quad + 2(\phi_5 + \phi_6 + \phi_7 + \phi_8) \\ &\quad + (\phi_9 + \phi_{10} + \phi_{11} + \phi_{12}) \end{aligned} \quad (3-16)$$

where  $h$  equals the distance between nodes and  $\nabla^4 \phi$  is the Airy stress function. The right-hand side of the equation defines a residual at the node in the center. This residual is obtained for each node in the mesh by assuming initial values for  $\phi$  at the nodes. After one set of calculations of  $\phi$  values in the mesh, the nodes obtained new values of  $\phi$  and the procedure is repeated until the iteration scheme converges. When this is reached all residuals approach zero.

Numerical results were obtained by Sturgul (1967) for a finite difference scheme applied to a rock wall. The various stress concentrations at the base of the rock wall were calculated. His study was instrumental in obtaining the directions and stress concentrations in the vicinity of a rock wall. But, as pointed out before, a finite element analysis will take into consideration the gravity effects. In addition, equal horizontal stresses can be applied on both vertical boundaries and their effect on the stress field examined.

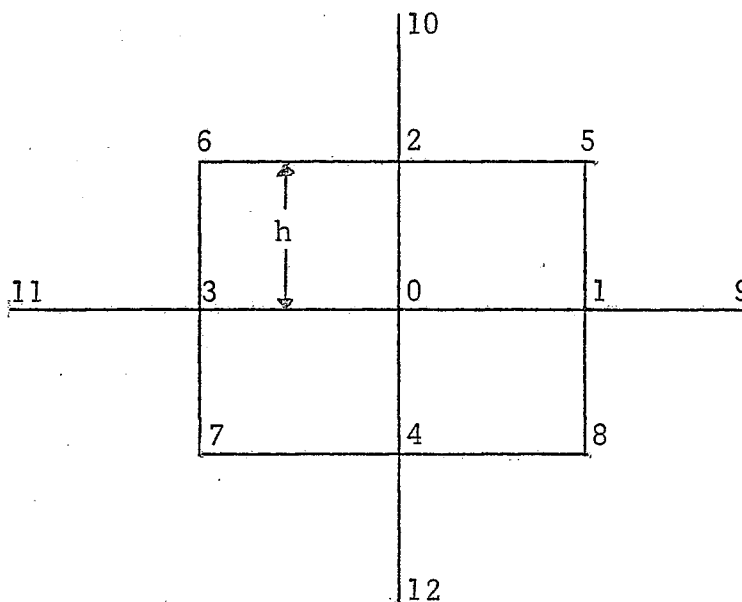


Figure 4. A mesh used in the solution of the finite difference approximation for the biharmonic equation

## CHAPTER 4

### THE FINITE ELEMENT METHOD

In all disciplines in the scientific world, a methodical research project starts out with a universal problem. The problem is then broken down to its components which are solved separately. Then all solutions of the parts are assembled to give the solution of the whole. This was the underlying idea behind the development of the finite element method. In practice, Turner et al. (1956) formulated the finite element method specifically for the design of aircraft structure.

#### The Concept of Finite Elements

The concept of the finite element method as first developed by Turner et al. (1956) involves the partitioning of a continuous solid into a finite number of elements interconnected by nodal points. The elements are assigned their physical properties of density, Poisson's ratio, Young's modulus and, in some cases, cohesive strength. In order to obtain the resulting deformation of such elements due to a wide variety of loading, a solution is obtained in the form of displacement values and stresses at the centroids of the elements. Having determined the stresses, the investigator can use appropriate criteria to predict possible failures.

A simpler, more accurate description of the method was given by Desai and Able (1972, p. 77), who wrote that the "basic philosophy of

the finite element method is piecewise approximation," or the treatment of discrete parts of a structure as simple and solvable mathematical matrices. The digital computer has advanced this technique to a practical and usable one.

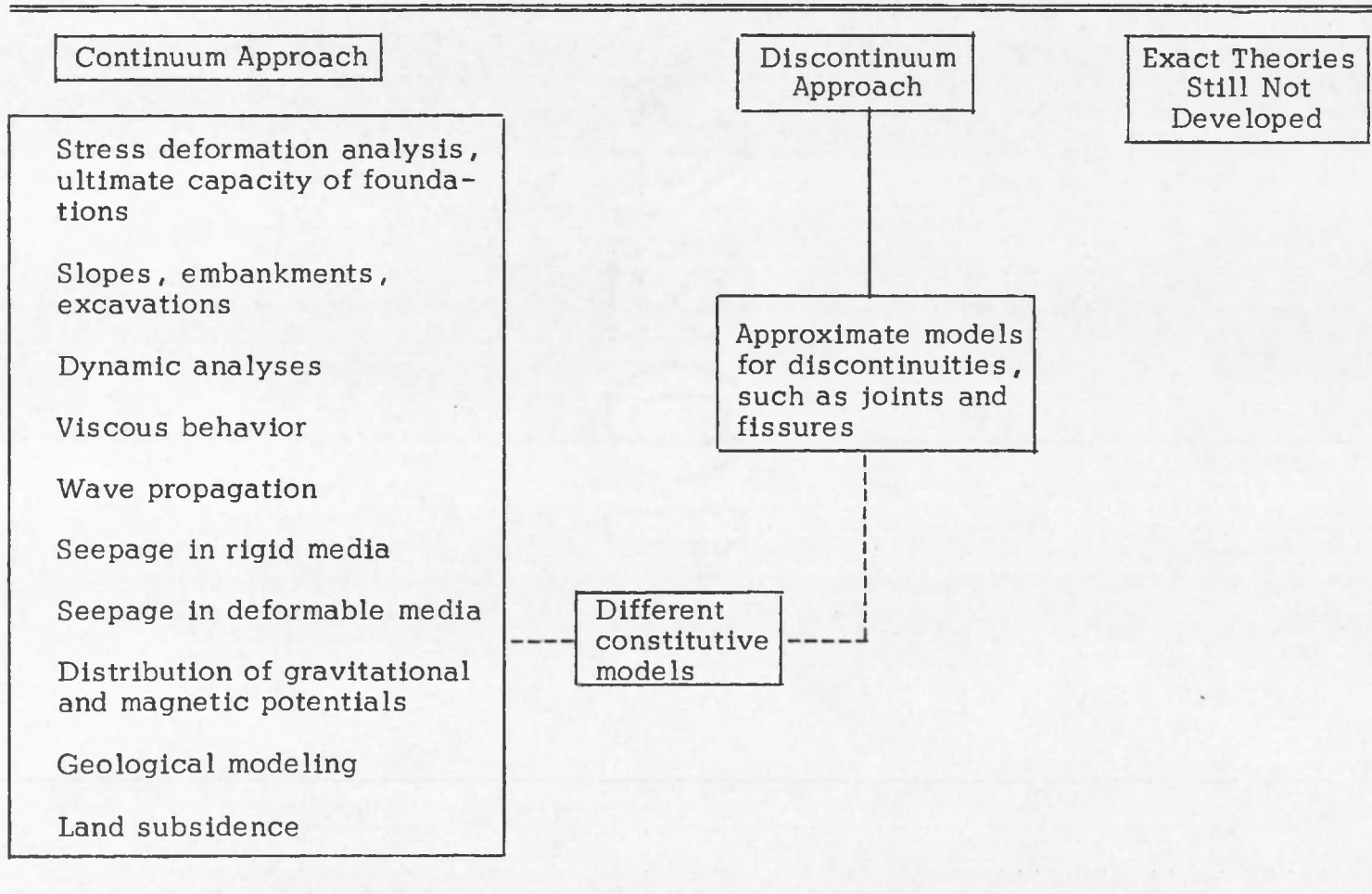
### Applications

Since its original development in the late 1950's for evaluation of aeronautical structural components, the finite element method has been used in other fields, such as rock mechanics (Clough, 1965, 1969), slope stability calculations (Hoskins, 1973), soil mechanics, and ship building. The more complete list of applications in geotechnical engineering given in Table 2 is from Desai (1972). One of the first applications to modeling geological structures was done by Voight and Samuelson (1969). The finite element method can be applied to a range of disciplines in the earth sciences, for example, geophysics, structural geology, geohydrology, geomorphology, glaciology, and engineering geology. Particular problems given to solution by this method are: behavior of rocks under static dynamic loading, seismic response, heat and fluid flow, and potential theory. Results of incorporating the effects of time have been made but on a restricted basis (Brischke, 1974).

The versatility of the finite element method as compared to classical mechanics is exhibited in its ability to be adapted to nonlinear systems. The material properties can be anisotropic and heterogeneous. There may even be structural discontinuities.

Desai (1972) pointed out in his paper on the state of the art the difficulties in applying the finite element method to geologic

Table 2. Applications of the finite element method to geotechnical engineering.--After Desai (1972)



materials; the major one is the multiphase nature of soil and rock. Characteristics that distinguish geologic material from man-made metals are discontinuities, such as fissures and joints, and residual stresses. Most of the geologic applications have adopted simple schemes of characterization. Even with this simplistic and sometimes approximative approach the method has been proved adequate to deal with geologic materials.

One of the pioneers to use the method was Douglas (1970), who pointed out the potential for using finite elements to model geologic structures. Stephansson (1973) and Hudleston and Stephansson (1973) modeled single-layer buckle folds where the stress is related to strain by the viscous flow law. This is one of the first examples of incorporating time into the stress-strain model.

Recently, two studies of the effect of stress release on the formation of new geologic structures have been completed at The University of Arizona. Sturgul and Grinshpan (1975) used the finite element method in their study of a two-dimensional cross section of the wall of the Grand Canyon, 7,750 m long and 4,500 m wide, to test a hypothesis proposed by Hamblin and Rigby (1969). The Hamblin and Rigby hypothesis was that the Muav Limestone, one of the formations in the Grand Canyon, has behaved elastically and the observed dip of 10 degrees away from the Colorado River is caused primarily by the stress relief when the overburden was removed by erosion.

The other study was by Lowenfels (1974). This study concerns itself with the restrained rebound of the earth that occurs when an ice sheet melts. The crustal dimensions used in this model were 50 km in

width and 30 km in depth; the ice load was 10 km thick. The removal of the ice sheet has resulted in a maximum rebound in the center of the area and tapers out 24 km away from the former edge of the sheet on either side.

### Theory

Several textbooks have been published on the subject of finite element analysis (Desai and Able, 1972; Martin and Carey, 1973; and Zienkiewicz, 1971). It is not the subject of this paper to describe the method of finite element analysis but to present justification for its use in study of the effects of horizontal stress on a rock wall and the body forces and displacement due to gravity. The general theory of using finite elements for plane stress analysis was presented by Clough (1960).

Basically, each individual element of a mesh is represented by a local stiffness matrix that consists of the coefficients of the equilibrium equations, determined by the material and geometric properties of the element. This is obtained by using the principle of minimum potential energy. The basic relationship between nodal point displacement and the elements are described linear algebraic equations generated by satisfying the equilibrium conditions at the nodes.

Using the notation given by Ural (1973) and standard notation from structural analysis, the basic equations are:

$$\{P\} = [A] \{Q\} \quad (4-1)$$

where.  $\{P\}$  = member-end forces

$[A]$  = load-force matrix

$\{Q\}$  = external loads.

$$\{U\} = [B]\{P\} \quad (4-2)$$

where  $\{U\}$  = member deformations

$[B]$  = force-deformation matrix.

$$\{D\} = [C]\{U\} \quad (4-3)$$

where

$\{D\}$  = node displacements

$[C]$  = deformation-displacement matrix.

The deformation-displacement matrix  $[C]$  is the same as the transpose of the load-force matrix:

$$[C] = [A]^T. \quad (4-4)$$

All algebraic equations are assembled into an overall global matrix representing the entire structure that also expresses the nodal equilibrium conditions:

$$\{Q\} = [K]\{\delta\} \quad (4-5)$$

where  $\{\delta\}$  = unknown nodal displacements. Equation (4-5) can be rearranged to be solved for the unknown nodal displacement  $\{\delta\}$  by finding the inverse of the stiffness matrix  $[K]$ .

The derivation of the nodal point displacement by the use of the finite element analysis is documented by Ural (1973, p. 90-93) and, as described by him, the fundamental principle of this analysis involves the total potential energy of the system ( $V$ ), which is given by

$$(V) = (U) - (U_P) - (U_R) - (U_S). \quad (4-6)$$

Each element of the above expression is described below.

Internal strain energy ( $V$ )

$$(U) = \frac{1}{2} \int_V \{e\}^T \{\sigma\} dV \quad (4-7)$$

where  $\{\epsilon\}^T$  = the transpose of strain  
 $\{\sigma\}$  = stress.

Equation (4-7) can also be expressed

$$(U) = \frac{1}{2} \int_V \{\epsilon\}^T [D] \{\epsilon\} dV \quad (4-8)$$

where  $\{\epsilon\}$  = strain vector.

$[D]$  = transformation matrix relating stress to strain, also known as the elasticity matrix.

Potential energy due to body forces ( $U_F$ ):

$$(U_F) = \int_V \rho \{\phi\}^T \{F\} dV \quad (4-9)$$

where  $\{F\}$  = body forces of the system

$\rho$  = mass density of the elastic body

$\{\phi\}$  = general displacement function.

Potential energy due to external nodal forces ( $U_R$ ):

$$(U_R) = \{\delta\}^T \{R\} \quad (4-10)$$

where  $\{\delta\}^T$  = transpose of nodal displacements

$\{R\}$  = external nodal loads.

Potential energy due to surface traction ( $U_S$ ):

$$(U_S) = \int_{\text{area}} \{\phi\}^T \{S\} dA \quad (4-11)$$

where  $\{\phi\}^T$  = transpose of general displacement function

$\{S\}$  = surface traction.

$A$  = area of a triangular element.

$\{\phi\}$  can be expressed as

$$\{\phi\} = \frac{1}{2A} \{N\} \{\delta\} \quad (4-12)$$

where  $N$  = a position matrix.

Equation (4-12) can be substituted in equation (4-11), which results in

$$(U_S) = \int_{\text{area}} \frac{1}{2A} \{\phi\}^T \{N\}^T \{S\} dA \quad (4-13)$$

Substitutions of equations (4-8), (4-9), (4-10), and (4-13) in equation (4-6) results in the following equation:

$$\begin{aligned} (V) = & \frac{1}{2} \int_V \{\epsilon\}^T D \{\epsilon\} dV - \int_V \rho \{\phi\}^T \{F\} dV - \{\delta\}^T \{R\} \\ & - \int_{\text{area}} \frac{1}{2A} \{\delta\}^T \{N\}^T \{S\} dA \end{aligned} \quad (4-14)$$

$\{\epsilon\}$  can also be expressed as

$$\{\epsilon\} = \{B\} \{\delta\} \quad (4-15)$$

where  $\{B\}$  = displacement strain matrix.

With substitution of equations (4-12) and (4-15) in equation (4-14), the following expression is obtained:

$$\begin{aligned} (V) = & \frac{1}{2} \int_V \{\delta\}^T \{B\}^T D \{B\} \{\delta\} dV - \int_V \frac{1}{2A} \rho \{\delta\}^T \{N\}^T \{F\} dA \\ & - \{\delta\}^T \{R\} - \int_{\text{area}} \frac{1}{2A} \{\delta\}^T \{N\}^T \{S\} dA. \end{aligned} \quad (4-16)$$

Equation (4-16) gives the total potential energy of one element. To obtain the total energy of all elements that make up a structure, equation

(4-16) is summed over all  $n$  elements and  $(V)$  is now

$$(V) = \sum_1^n f(x) \quad (4-17)$$

where  $f(x)$  is total potential energy of one element expressed by equation (4-16).

Nodal displacements  $\{\delta\}$  are not related to the  $x$  and  $y$  coordinates and can be taken out of the integrals of equation (4-16):

$$\begin{aligned} (V) = \sum_1^n & \left[ \frac{1}{2} \{\delta\}^T \int_V \{B\}^T \{B\} dV \cdot \{\delta\} \right. \\ & - \{\delta\}^T \int_V \frac{\rho}{2A} \{N\}^T \{F\} dV - \{\delta\}^T \{R\} \\ & \left. - \{\delta\}^T \int_{\text{area}} \frac{1}{2A} \{N\}^T \{S\} dA \right] \quad (4-18) \end{aligned}$$

The last three terms of equation (4-18) represents the total loading system  $\{Q\}$  of the analysis:

$$\begin{aligned} \{Q\} = \sum_1^n & \int_V \frac{\rho}{2A} \{N\}^T \{F\} dV + \{R\} \\ & + \int_{\text{area}} \frac{1}{2A} \{N\}^T \{S\} dA \quad (4-19) \end{aligned}$$

Therefore equation (4-18) can be written:

$$(V) = \sum_1^n \frac{1}{2} \left\{ \{\delta\}^T \int_V \{B\}^T [D] \{B\} dV \cdot \{\delta\} \right\} - \{\delta\}^T \{Q\}. \quad (4-20)$$

The stiffness matrix  $[k]$  of an element is expressed as

$$[k] = \int_V \{B\}^T [D] \{B\} dV \quad (4-21)$$

and the total stiffness matrix  $[K]$  over the range of  $(V)$  is

$$[K] = \sum_1^n [k]. \quad (4-22)$$

Substituting equation (4-22) in equation (4-20) gives

$$(V) = \sum_1^n \frac{1}{2} \{\delta\}^T [k] \{\delta\} - \{\delta\}^T \{Q\}. \quad (4-23)$$

Under the principle of stationary potential energy, the equilibrium conditions are satisfied when the potential energy is minimum. This is satisfied when the derivatives of the unknown nodal displacements vanish.

$$\frac{\partial V}{\partial \delta_1} = \frac{\partial V}{\partial \delta_2} = \frac{\partial V}{\partial \delta_3} = \dots = \frac{\partial V}{\partial \delta_n} = 0 \quad (4-24)$$

Therefore equation (4-23) can be written as:

$$[K] \sum_1^n \{\delta\}_n = \{Q\} \quad (4-25)$$

and

$$\sum_1^n \{\delta\}_n = [K]^{-1} Q \quad (4-26)$$

where  $\{\delta\}_n$  = one nodal displacement.

Once the nodal displacements

$$\{\delta\} = \sum_1^n \{\delta\}_n \quad (4-27)$$

are obtained, the strain can be calculated from equation (4-15)

$$\{\epsilon\} = [B] \{\delta\}$$

and the stress is computed by:

$$\{\sigma\} = \begin{Bmatrix} \delta_x \\ \delta_y \\ \tau_{xy} \end{Bmatrix} = [D] \begin{Bmatrix} \epsilon_x \\ \epsilon_y \\ \nu_{xy} \end{Bmatrix} \quad (4-28)$$

where  $\tau_{xy}$  is the shearing stress in the  $y$  direction and  $\sigma_x$  and  $\sigma_y$  are the stresses in the  $x, y$  directions;  $\epsilon_x$ ,  $\epsilon_y$ , and  $\nu_{xy}$  are strains in the  $x, y$  directions. Equation (4-28) can be written in a general form as:

$$\sigma = [D] \{\epsilon\}, \quad (4-29)$$

which is the more familiar Hooke's law.

In treating some linear problems it is necessary to introduce a factor that accounts for the plasticity effects. One way was proposed by Isakson, Armen, and Pifko (1967). They suggested introducing initial stresses or strains to the matrix equation governing elastic structural behavior.

The treatment of other variations from linearity, such as bilinear or nonlinear time-dependent or temperature-dependent properties of anisotropic and viscoelastic materials, are mathematically more complex. For the mathematical expressions of these variations, the reader is referred to the references mentioned in this chapter.

## CHAPTER 5

### GENERAL FORMULATION OF A FINITE ELEMENT MODEL

In the formulation of a finite element model we recognize several stages. The first stage is the physical collection of data for the material properties, such as Young's modulus, density, and Poisson's ratio, or the assignment of values to them. Normally, such data are obtained from a stress-strain curve derived from experiments done in the laboratory or from field measurements. This stage is by far the most important since the principle behind the construction of a mathematical models is the approximation of the actual physical conditions as close as possible. In pursuing this idea it is necessary to determine if the rock behavior can be expressed by Hooke's law, which states that stress and strain are proportional, or if it is nonlinear.

One rarely finds materials in nature that behave isotropically, but if it does not provisions can sometimes be made. Serious errors in calculated stress field and deformation can occur due to ignoring residual stresses existing in the rocks. This can be handled by the finite element method by the process of incremental loading and unloading rather than loading and unloading the complete unit mass all at once.

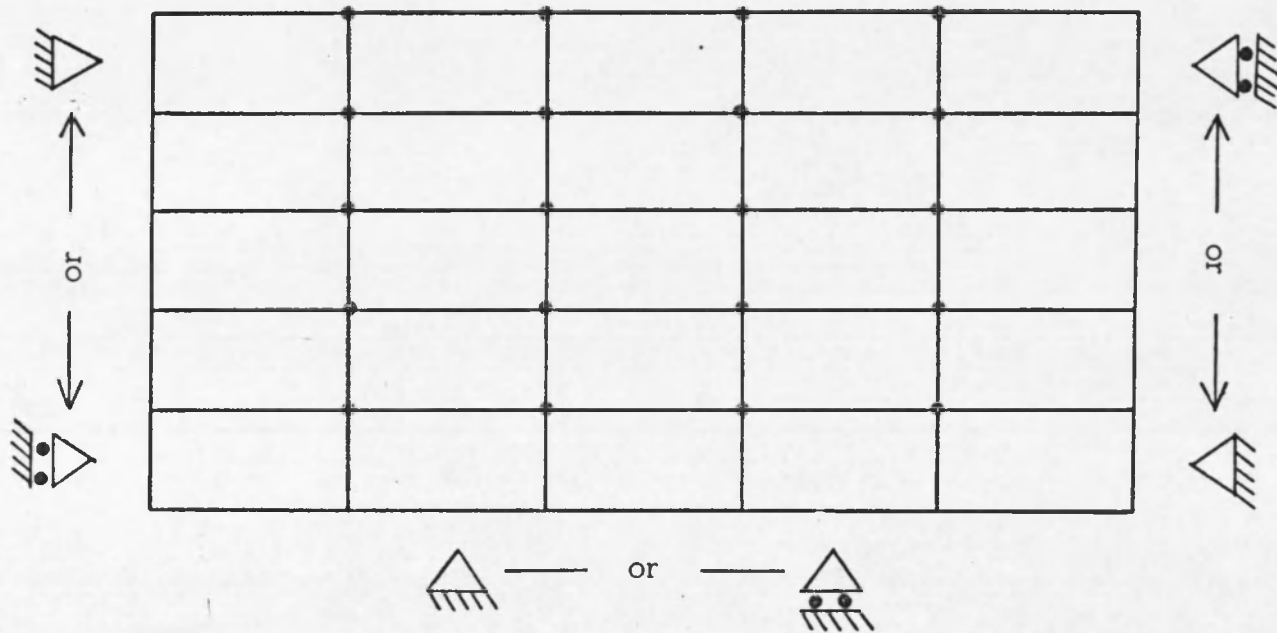
All the models in this thesis were considered to consist purely of elastic materials behaving isotropically without residual stress.

The next step is superimposing a mesh and determining the boundary conditions. The mesh outline can be visualized as a

two-dimensional stratigraphic cross section. The stratigraphic continuum is then subdivided into an assemblage of finite elements, which can be either rectangular or triangular. Where the boundaries are irregular or where more detailed information about the stresses is desired, a finer mesh is constructed. The finer the mesh, the closer the approximation is to the accurate solution. This involves an increase in the number of elements and nodes and therefore an increase in computer expense. A realistic approach is a compromise that will keep the expenses down and still yield a reasonable accuracy. In using a modern digital computer one must always keep in mind the two major limitations: storage space and expense.

Many engineered bodies studied in structural mechanics possess well-defined geometries with known boundaries. Most geological bodies involve very large bodies without well-defined boundaries. To make such geological bodies amenable for discrete analysis it is necessary to idealize the body. This is achieved by limiting the boundaries of a continuum. In order not to force solutions by arbitrary boundary conditions, it is necessary to determine boundaries at a distance where they have no effect on the solution. The determination of this distance may have to be arrived at by trial and error. The boundary nodal points can be set so that they are free to move in any direction in an  $x,y$  plane or are limited to movement in the  $x$  or  $y$  direction only (Fig. 5).

The last stage is the computed solution, which is given in terms of displacement of nodal points, amplitude and direction of stress of the element centroid, possible failure locations, and tensile stress.






- 
- Movement permitted in one direction
- 
- Fixed
- 
- Free to move in all directions

Figure 5. Boundary conditions

### Computer Programs

To obtain a finite element solution for a problem having many elements, data were fed into a main program and the solution obtained numerically. However, four other programs were used to assist in the formulation of the model and to obtain a solution in the form that was best suited for analysis and interpretation.

A program was used as a debugging device to locate possible mistakes in coordinates and numbering of nodes and elements. Each node and element requires a separate punched card; hence the possibility of error in the data cards is great. An added advantage of using this program is that the computer can draw a plot of the user's model on a CALCOMP plotter to the user's specifications.

A mesh generator was the first program used in the sequence. The next program minimized the maximum nodal point difference for the elements of the model. The output of this program is given in two forms: (1) numeric output, which simply numbers the nodal points in such a way that the maximum nodal-point difference around the elements is minimized, and (2) punched data cards with the revised numbering of the nodes ready for input in the main program. By minimizing the maximum nodal-point difference, this program decreases the time necessary to run the main program and increases the capacity for a larger array of nodes and elements.

If all elements are rectangular and all boundaries smooth, a much more efficient method is to use a newly devised program to generate the mesh. This program produces a mesh and a punched output in a form that optimizes the numbering of the nodes. This program was used

successfully in the solution of the rock-wall problem, but it was necessary to use the longer route for the Alpine problem because of the triangular elements and irregular boundaries.

The last program used is designed to present the solutions obtained by the main program in several different forms. This program uses the CALCOMP plotter. It was used in this project to illustrate the direction and relative amount of displacement at each nodal point; to obtain maximum and minimum principal stress directions and magnitudes at the centroid of each element; to obtain the numerical value of the principal stresses as well as of the shear stresses at the centroid of each element. The last is useful for contouring. It was also used to check the stability of each element by applying the Mohr criteria. The plots are in Appendix C.

## CHAPTER 6

### APPLICATION OF FINITE ELEMENT MODELS TO THE STUDY OF STRESS FIELDS

Finite element models were formulated to study indirectly the stresses in the interior of a mountain mass and to study the effect of the horizontal component of the earth stress field on and around a rock-wall structure.

#### Finite Element Model of an Alpine Cross Section

A single detached mountain massif, the Hochkönig massif, was chosen as the area of investigation. It is located on the southern edge of the northern calcareous Alps in Salzburg Province, Austria, at about lat  $47^{\circ}27'$  N. and long  $13^{\circ}07'$  W. (Fig. 6). A view of the terrain looking north is shown in Figure 7.

The basement of the massif comprises a series of metamorphic Paleozoic graywackes underlying a sequence of Triassic sedimentary rocks. Table 3 shows this sequence of layers. A schematic geological cross section trending north-south is given in Figure 8.

#### Formulation of the Model

The outline for the model is taken from a north-south cross section (Fig. 8) of the Hochkönig massif. The cross section is 5,000 m along the abscissa and 1,500 m along the ordinate, and starting at 1,000 m above sea level rises to 2,500 m.

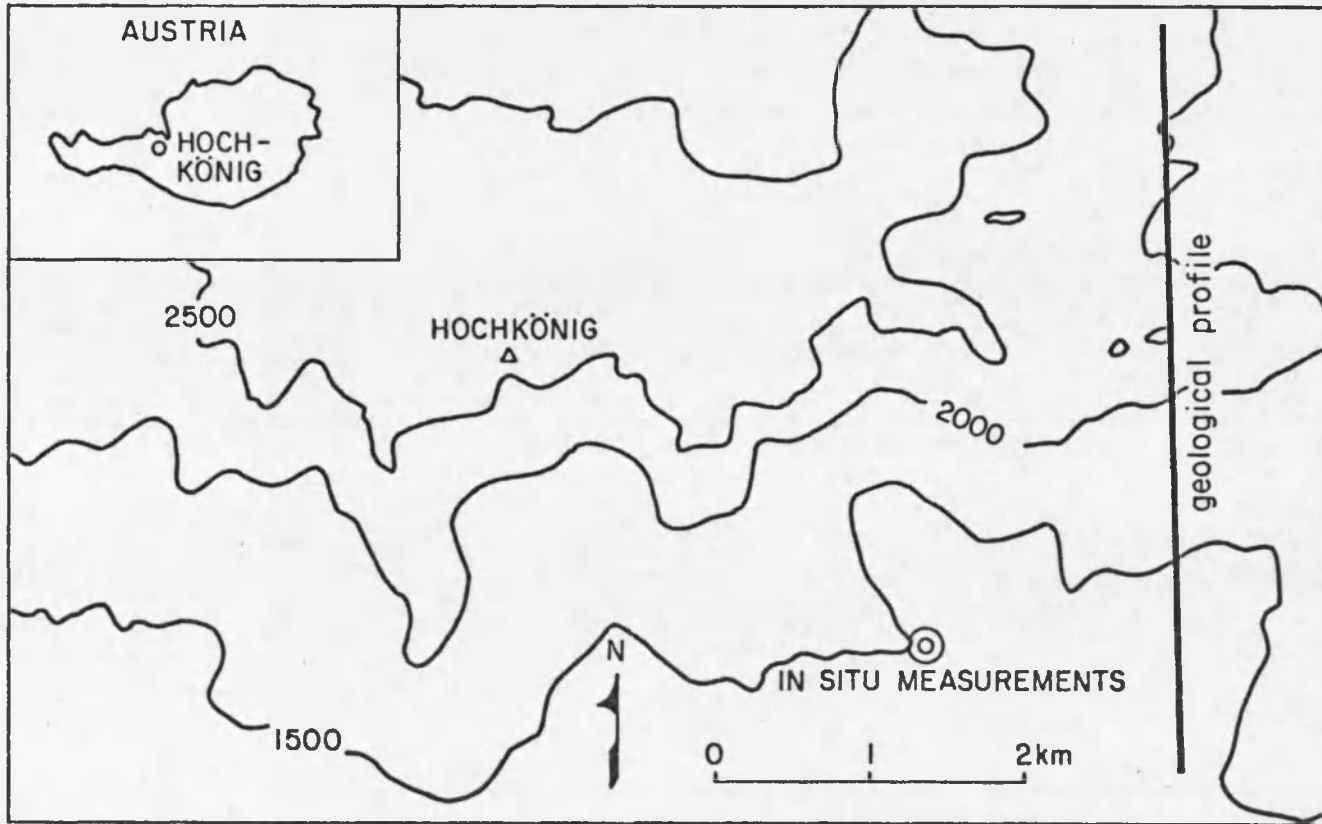


Figure 6. Location map of Hochkönig massif and position of geological profile



Figure 7. View of the terrain of the Hochkönig massif, looking north

Photograph courtesy of A. E. Scheidegger.

Table 3. Sequence of layers in the Hochkönig area

Triassic	Dachstein Limestone (Rhat)	Coral reefs
	Main Dolomite (Nor)	(phenomenologically like Ramsau Dolomite)
	Raibl Layers (Karn)	black shale, thin foliation, interspaced with dolomite and limestone
	Ramsau Dolomite (Ladin)	
	Gutenstein Dolomite (Anis)	dark blue gray dolomite with white veins of feldspar
	Werfen Layers (Buntsandstein) (Shyth)	reddish to yellowish sand- stones and quartzites, red to brown-yellow arenaceous slates; foliate conglomerates at base
Paleozoic	Graywackes	
	Green Series (Pern)	green argillaceous slates and quartzites
	Purple Series	purple phyllites, reddish to purple quartzites, conglom- erates, and arenaceous slates
	Gray Series (Pinzgau phyllites)	dark-gray phyllites, light- colored quartzite phyllites, light-colored sericite slates

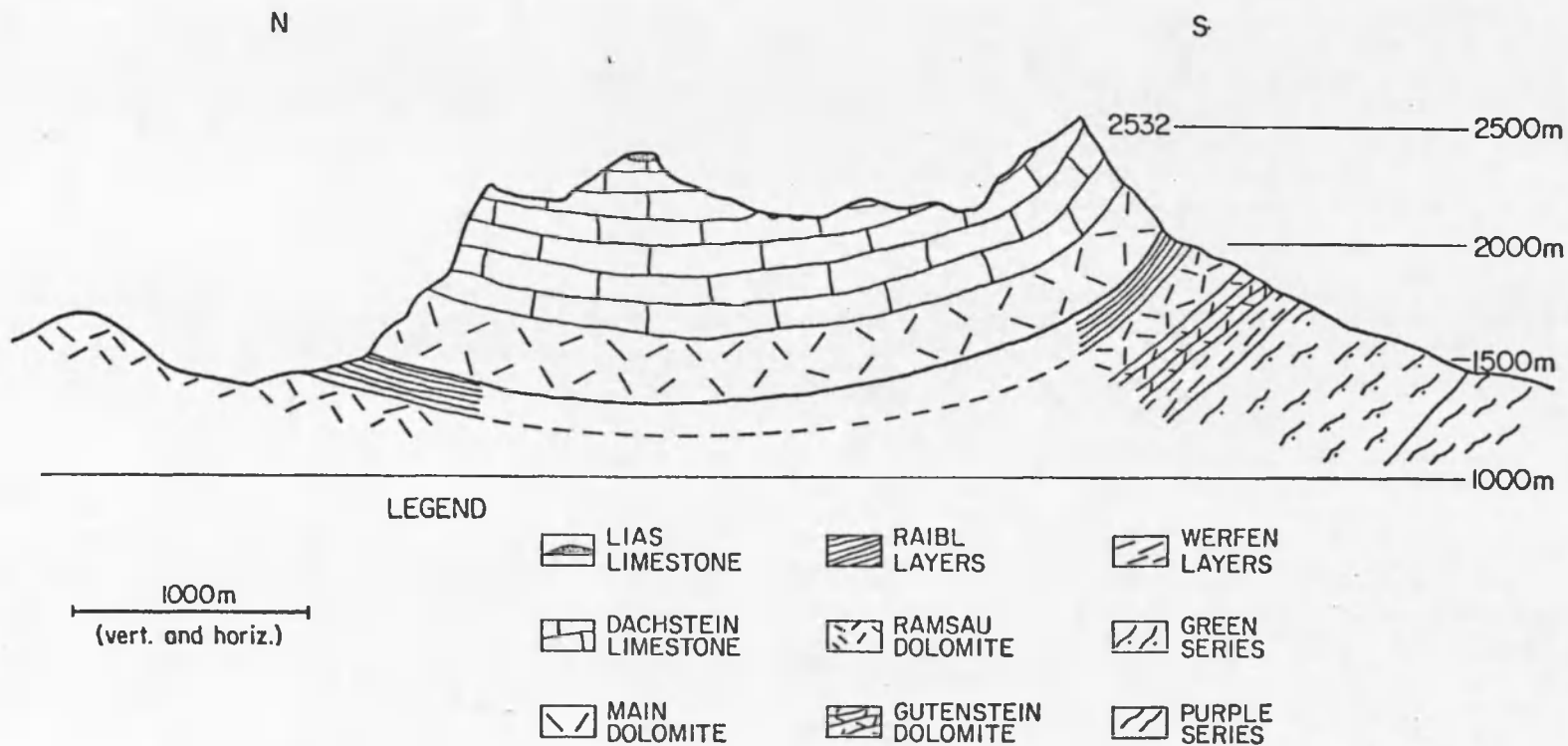


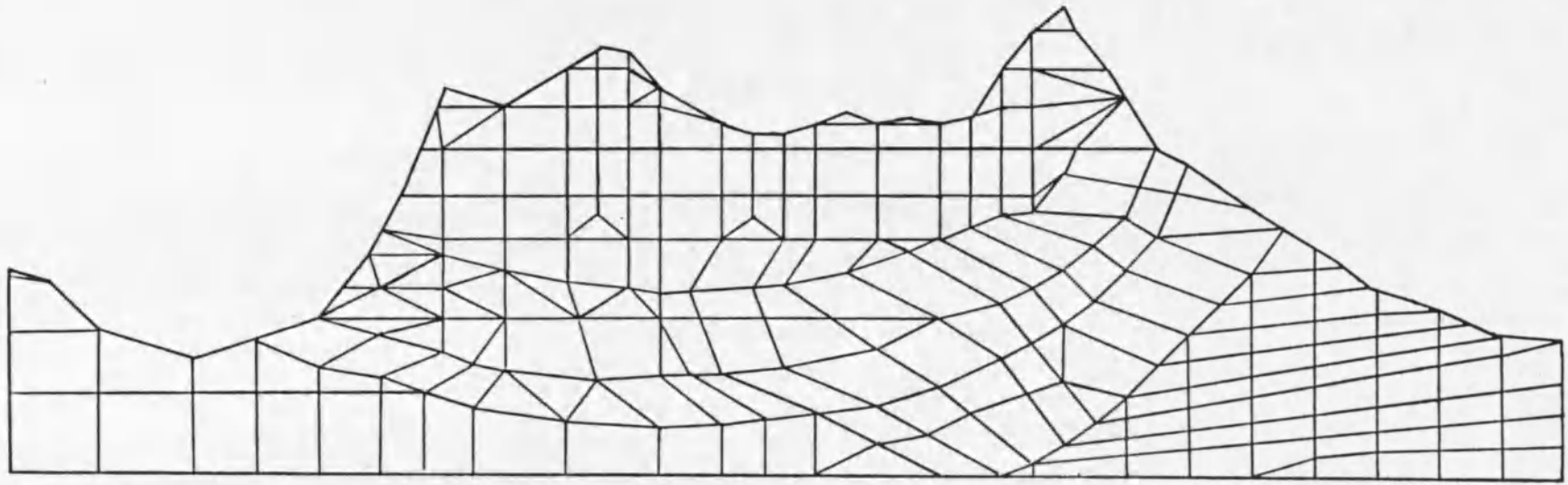
Figure 8. A north-south geological cross section of the Hochkönig massif

The cross section was subdivided into four stratigraphic layers, and each layer was further subdivided into triangular and quadrilateral units, as shown in Figure 9. These are the finite elements. Values for Poisson's ratio, Young's modulus, and density were assigned for each element. These values were determined from actual field investigations and were obtained from A. E. Scheidegger (written commun., 1975). They are believed to be accurate. Each separate layer was assumed to have constant physical properties; therefore, all elements in a layer were assigned the same values for the physical properties. These values are given in Table 4.

Table 4. Values for physical properties of the Hochkönig layers

Layer	Young's Modulus	Poisson's Ratio	Density (g/cm <sup>3</sup> )
Dachstein Limestone Lias Limestone	640 x 10 <sup>3</sup> kg/cm <sup>3</sup>	0.21	2.5
Main Dolomite Ramsau Dolomite Gutenstein Dolomite	320	0.21	2.5
Raihl Layers	110	0.34	2.5
Werfen Layers Graywackes (Green and Purple Series)	240	0.34	2.7

In order to satisfy the compatibility relations, some of the nodal points had to be constrained in freedom of movement. All nodes inside the model could move in any direction. Those along the left and



1000 m  
Vertical and horizontal

Figure 9. Finite element model of Alpine cross section

right sides were confined to move up and down but not horizontally; those along the base could move only horizontally. The two corner nodes along the base were fixed.

### Discussion

Using a simple contouring system for the maximum principal stresses in the Hochkönig massif (Fig. 10), it becomes clear that the greater stresses are under areas of high relief. Furthermore, the stress gradient along the steep slopes is greater than in the interior. The minimum principal stress is very small and oriented parallel to the slopes at locations close to the slopes. This part must be conceived intuitively because the small and large magnitude minimum principal stresses are so randomly distributed in the interior of the massif that they could not be contoured. The magnitude of the shear stresses influences the location of failure points along the slopes. It is therefore imperative when studying physical erosional phenomenon to look at the shear-stress concentration along a slope. Figure 11 shows an increase in magnitude of the shear stresses downslope, with the greatest magnitudes between one-third and two-thirds downslope and a decrease toward the bottom. These data can be used to predict exactly where creep may be started due to high shear-stress concentration.

In one of the programs, the Mohr criteria were applied. These make use of the principal stresses (Fig. 12) to calculate and to obtain a graphic figure of stable and unstable elements, as shown in Figure 13. This program determines whether shear stresses in an element have exceeded the maximum shear stress of the material. In Figure 13, a plus sign or triangle is drawn in the centroid of an element to indicate the

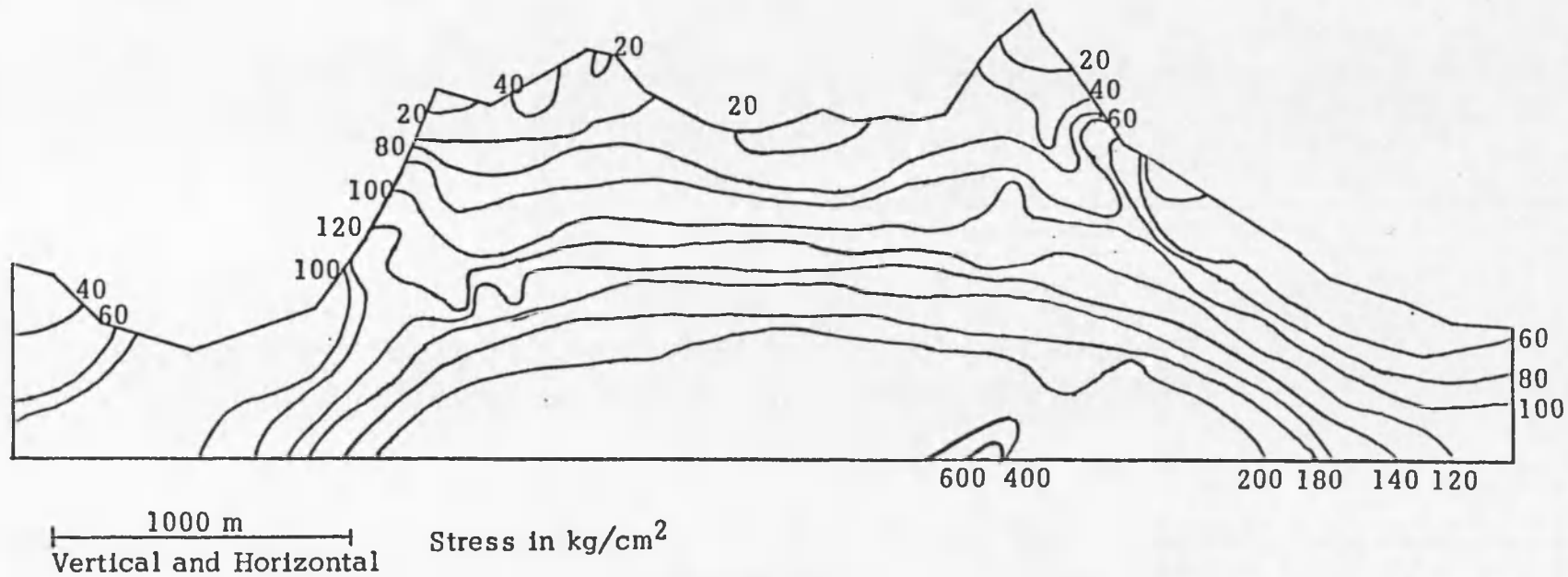


Figure 10. Maximum principal stress contours for Alpine cross section

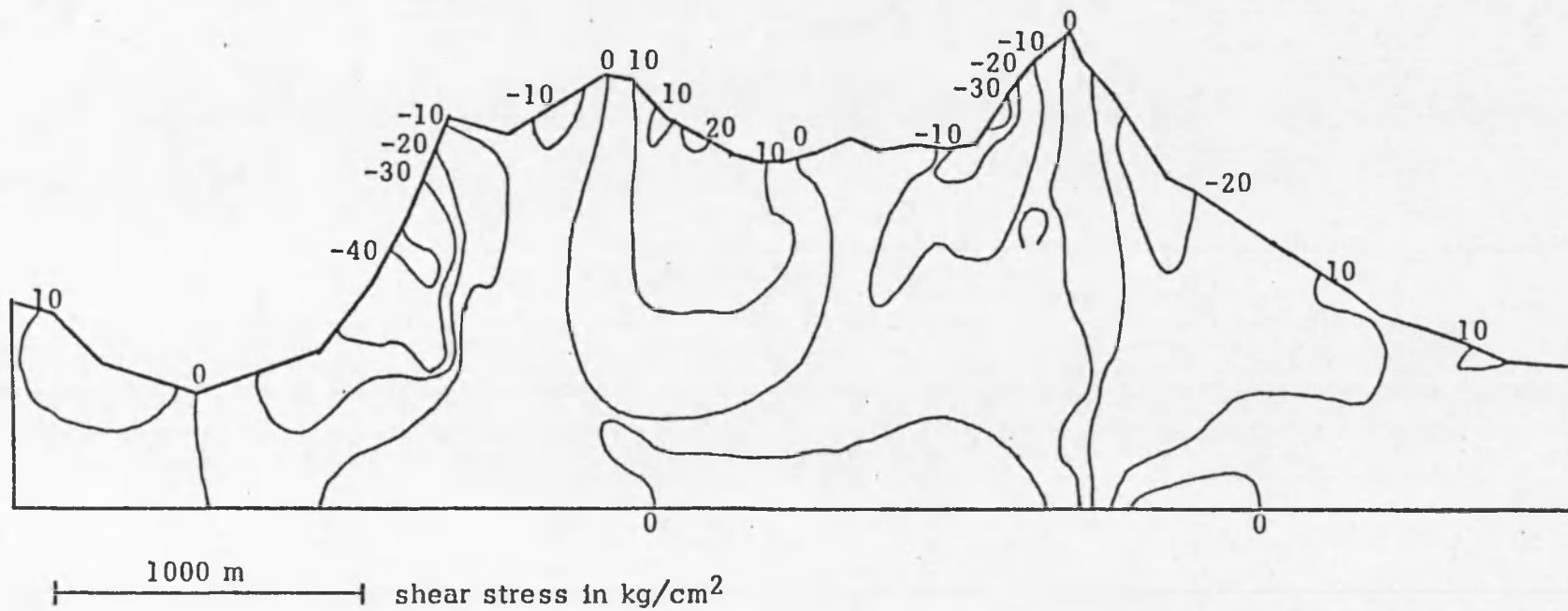
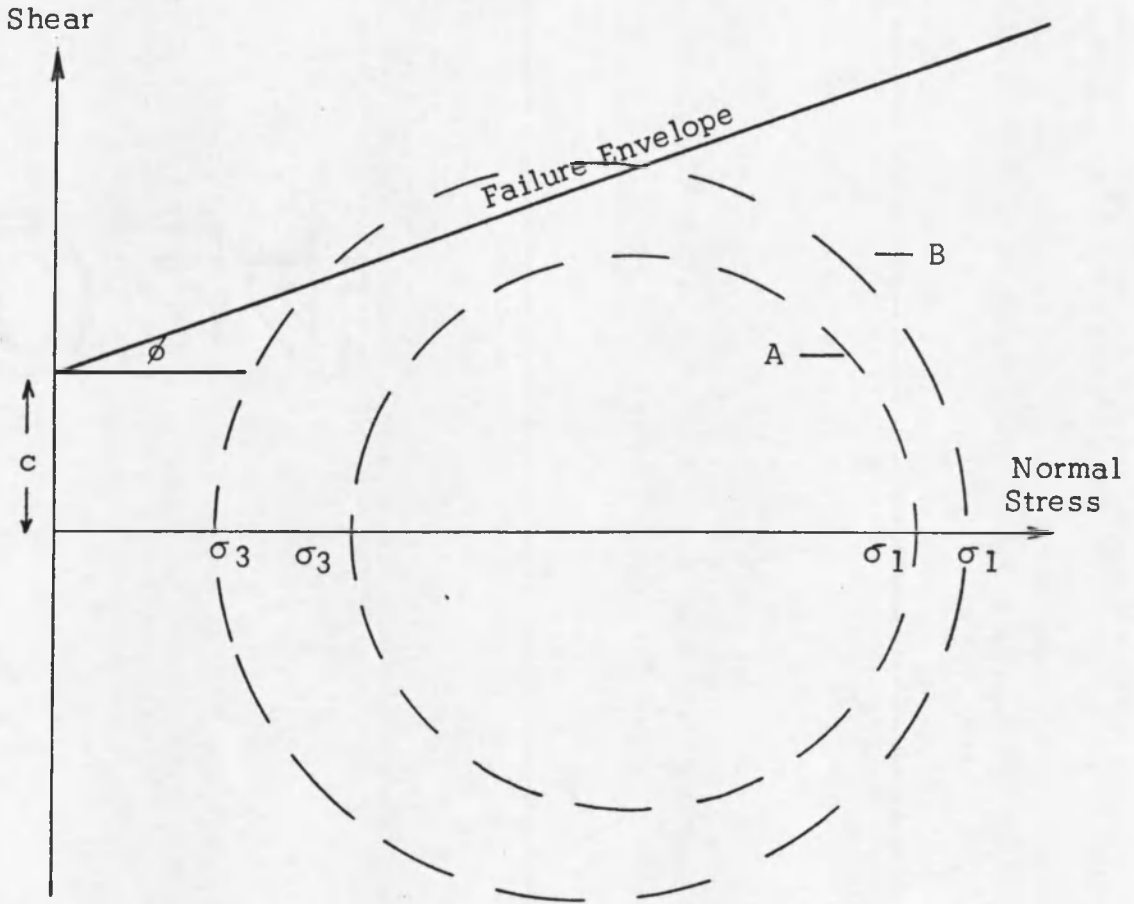


Figure 11. Vertical component of shear stress for Alpine cross section



$c$  = cohesion

$\phi$  = angle of internal friction

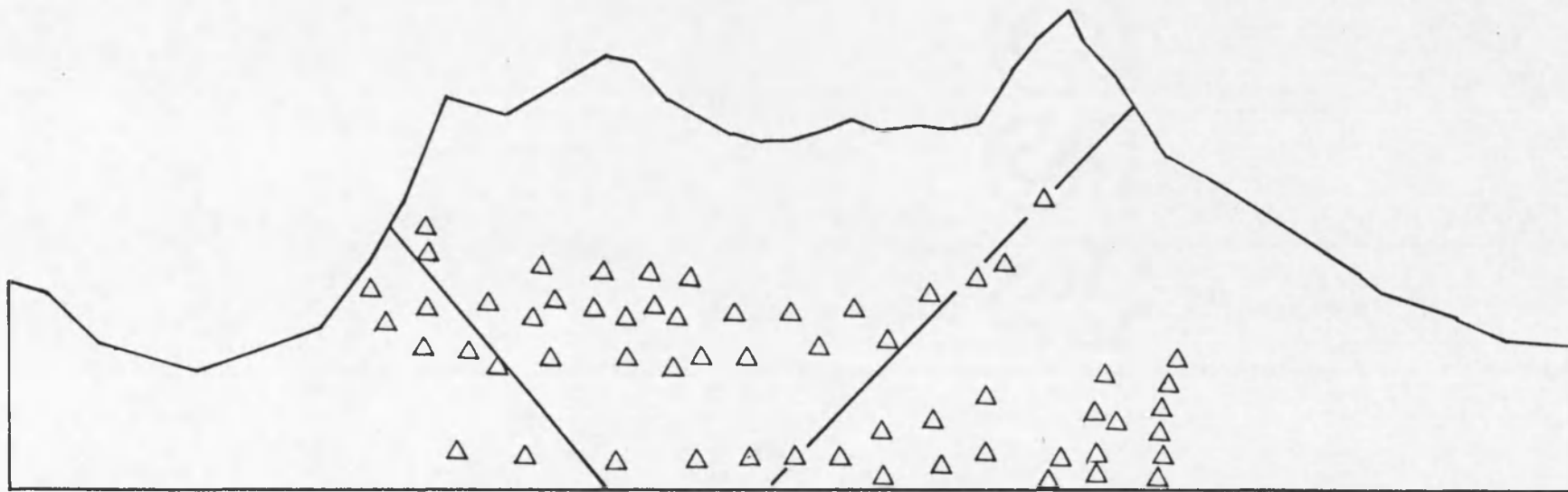
$\sigma_1$  = maximum principal stress

$\sigma_2$  = minimum principal stress

A = describes a stable element; does not pass through the failure envelope

B = describes an unstable element; passes through the failure envelope

Figure 12. Mohr failure criteria



1000 m  
 Vertical and Horizontal

△ unstable elements  
 \ / conjugate fracture  
 empty space indicates stable element

Figure 13. Conjugate fracture system for Alpine cross section

stability or instability, respectively, of the element. Another physical property, cohesion, is necessary in order to obtain the true failure of a material by this method. The cohesion for the different layers was not available for this study and an estimated value was therefore used. Figure 12 shows a fracture occurring about half way downslope and a system of conjugate fractures developing directly under the maximum load area.

The conjugate fractures may not be physically developed if the confining stress in the x,y directions is large enough. Such is not true of a section exposed to the atmosphere, such as along a slope. In this section, the loading due to gravity creates conjugate lines of weakness or fracture. This supports the Gerber and Scheidegger (1969) hypothesis that states that some of the V-shaped gullies and valleys are stress-induced features or, at least, the outline of such was marked by stress and the removal of material was performed by more conventional means, such as atmospheric and fluvial agents.

The fracture on the north slope of the cross section (Fig. 13) occurs at an area corresponding to Zone II, which was discussed in Chapter 2. Furthermore, on top of the slope the area that corresponds to Zone I (Ampferer, 1939) proves to be numerically in agreement with the area hypothesized by Ampferer to be the area of tensile stress (Fig. 14). The finite element solution shows the tensile stress to be maximum next to the slope as indicated by the minimum principal stress acting in the opposite direction.

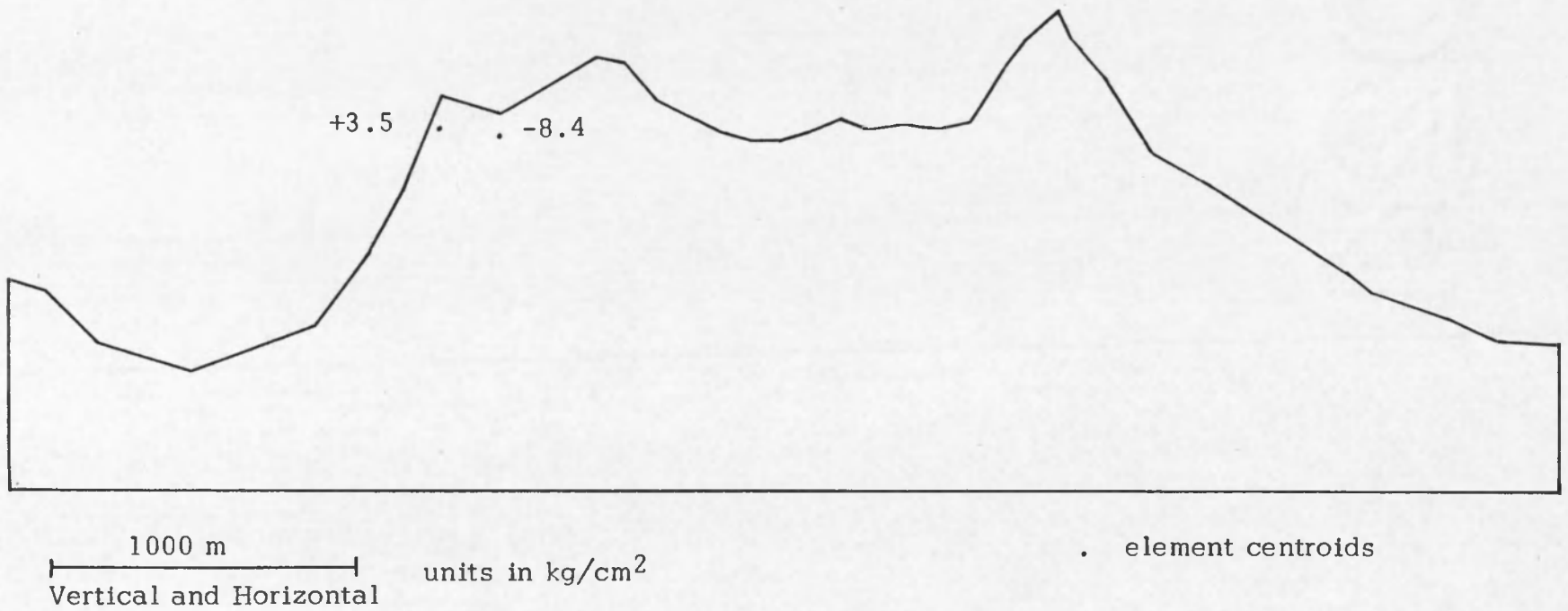


Figure 14. Stresses acting in opposite directions creating tensile stress for Alpine cross section

## Finite Element Model of a Rock Wall

### Formulation of the Model

A two-dimensional cross section of a vertical wall was considered. The dimensions assigned to this theoretical model are width 600 feet, height on the far right 400 feet and height on the far left 310 feet. The notch is 90 feet high and 300 feet away from each boundary side. The height of the notch is relatively small compared to its distance from the model's boundaries so that the study will be confined exclusively to the influence on the rock wall of the stress field next to it without boundary effects.

The cross section was subdivided into three stratigraphic layers, each of which was further subdivided into quadrilateral elements as shown in Figure 15. As in the massif problem, values were assigned to Poisson's ratio, Young's modulus, and density for each layer, as given in Table 5, and each layer was assumed to have constant physical properties. The values assigned are those for real rocks but not for any particular area of study.

Table 5. Values assigned for physical properties for the rock-wall model

Layer	Young's Modulus (psi)	Poisson's Ratio	Density (lb/in. <sup>3</sup> )
Material 1 (at base)	$0.3 \times 10^7$	0.2	0.095
Material 2 (at base of notch)	.2	.22	.092
Material 3 (on top)	.1	.26	.090

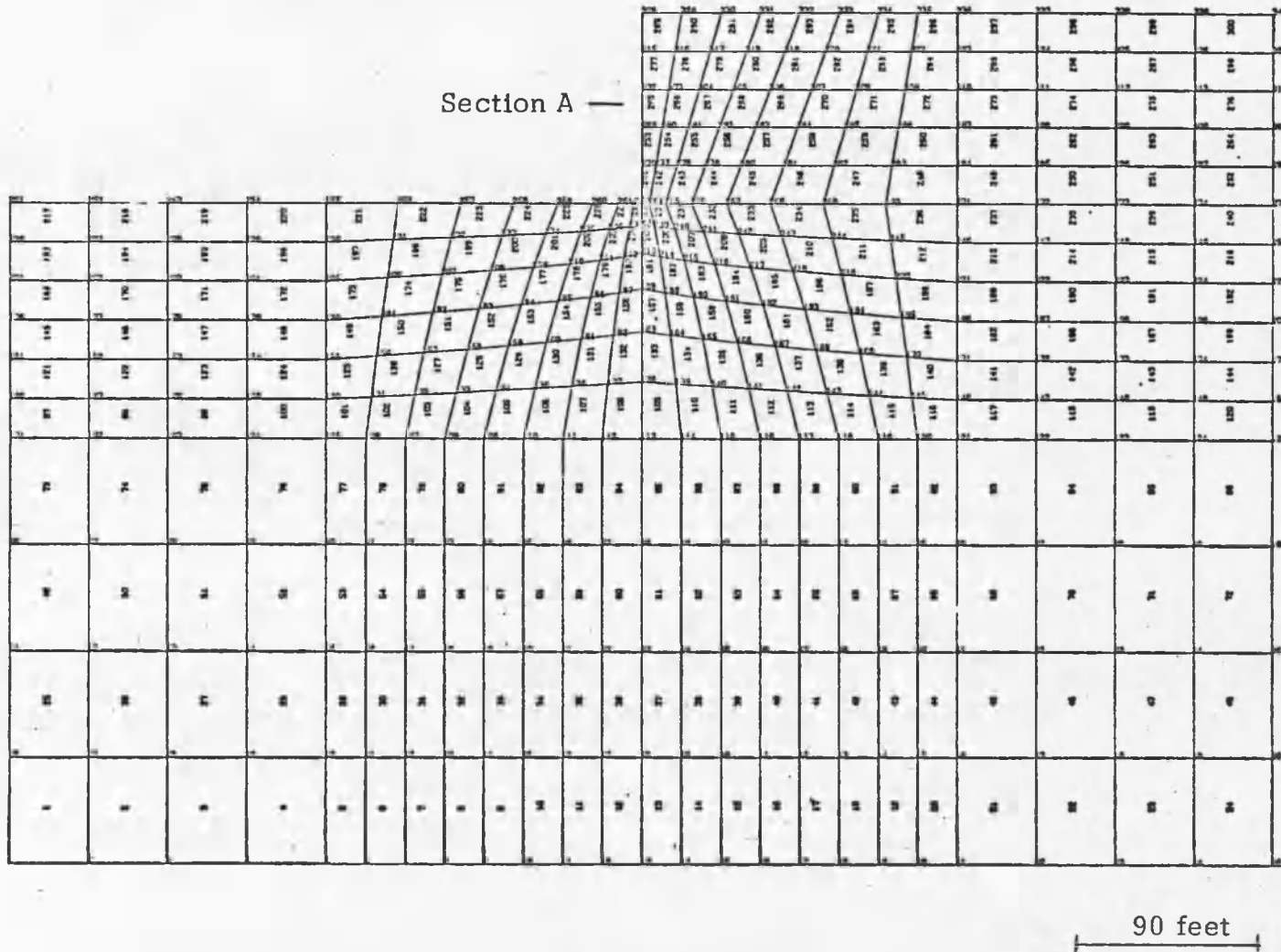


Figure 15. Finite element model of rock wall

Two different boundary restrictions were set. For the model subjected to gravity alone, the nodes were set as described for the massif model. For the model acted upon by horizontal stress (tectonic stresses), the nodal-point restrictions were: the center of the base line is fixed; the rest of the nodes on the base can be thought to be on rollers moving only horizontally; all other nodes in the model are free to move in all directions.

In one case, the horizontal stress applied to one side of the wall was equal but opposite in direction to the horizontal stress applied to the other side. The values for the horizontal stress for the right side ( $\sigma_H$ ) were calculated from the following equation:

$$\sigma_H = \frac{\nu}{1 - \nu} \sigma_V \quad (6-1)$$

where  $\nu$  is Poisson's ratio and  $\sigma_V$  is vertical stress. An equal but opposite stress component was applied to the left side (Fig. 16).

In another case, illustrated in Figure 17, the horizontal stresses for each side of the rock wall were calculated separately using equation (6-1).

### Discussion

The different methods for presenting numerical data are listed in Appendix C. For this thesis the simple contouring method was chosen because it highlights steep stress gradients and strong stress concentrations.

It is worthwhile to note at the beginning of this discussion that there is very little difference between the principal stresses acting near

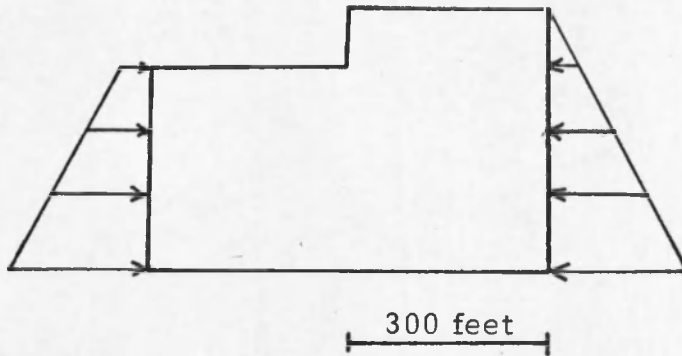


Figure 16. Rock wall with horizontal stress equal and opposite

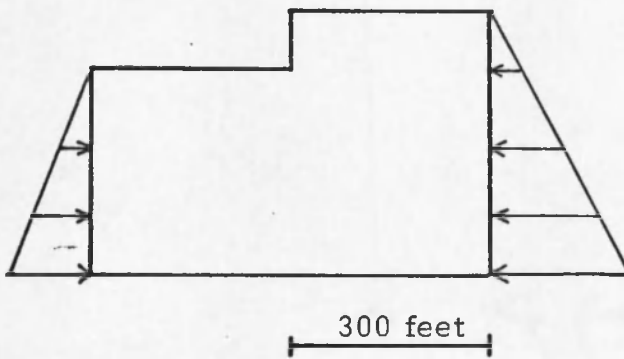


Figure 17. Rock wall with horizontal stress calculated separately on each side

a rock wall solely under gravity and stresses after application of horizontal stress. Therefore, what is said here applies equally to both cases unless otherwise stated.

The principal stresses in most of the domain ( $\sim 90\%$ ) are not affected by the notch and are nearly horizontal or vertical. The magnitude of the maximum principal stress is a function of the overburden. As shown on Figure 18, the angle of the maximum principal stress with the horizontal is 45 degrees under the notch; going to the left away from the notch the angle increases to 90 degrees and greater. At the notch the difference between the maximum and minimum principal stresses is maximal. As evident from Figure 12, the difference between the maximum and minimum principal stresses dictates failure or no failure, given a constant cohesion and  $\phi$ . Along the wall, the upper one-third shows tensile stresses acting upon it.

A comparison between Figures 18, 19, and 20 shows that the high value for the maximum principal stress is concentrated exactly at the notch. That means that horizontal stress, even when not applied equally and opposite, will have the same approximate effect on the maximum principal stress at the notch. This is not the case with the minimum principal stresses. The three figures show that the horizontal stress in addition to the obvious higher stress values next to the notch also creates a high at about two nodes to the right of the notch. The complete significance of the high stress value here is not utterly clear, but if the Mohr criteria were used this would mean that the high minimum principal stress with no change in the maximum principal stress would cause higher stability at this point.

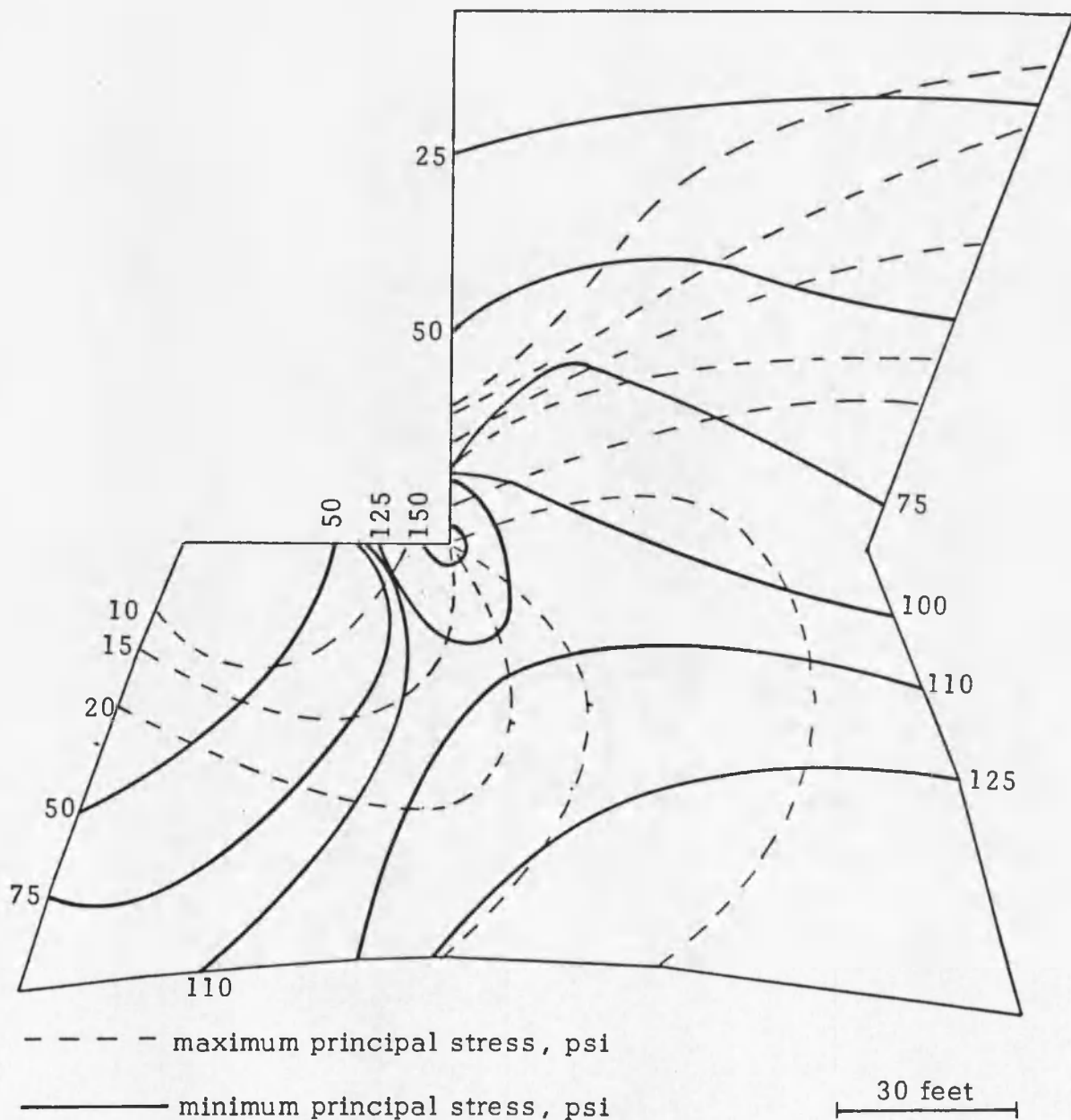


Figure 18. Maximum and minimum principal stresses, section A of rock-wall mesh, no horizontal stress applied

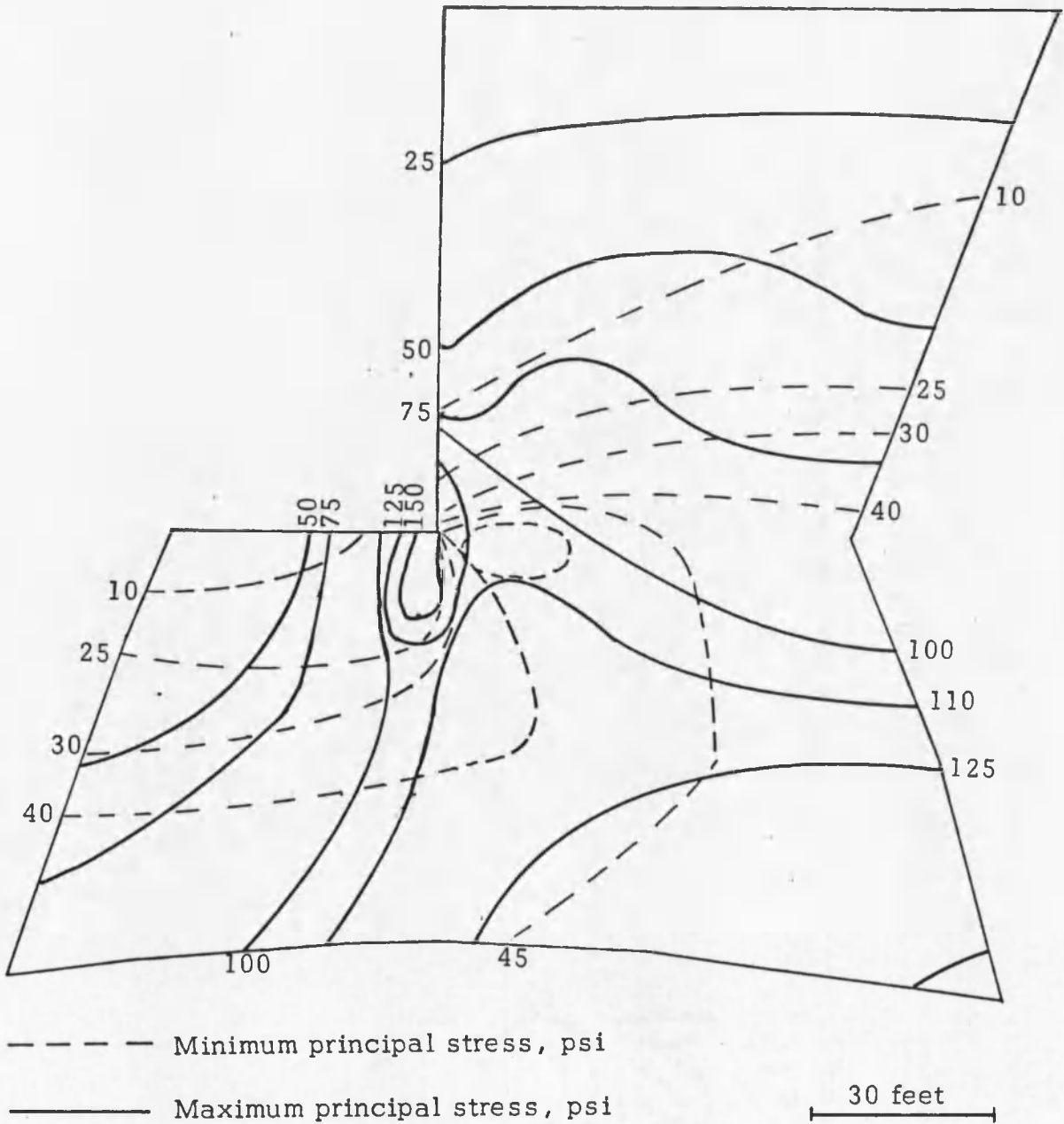


Figure 19. Maximum and minimum principal stresses, section A of rock-wall mesh, applied horizontal stress, equal and opposite

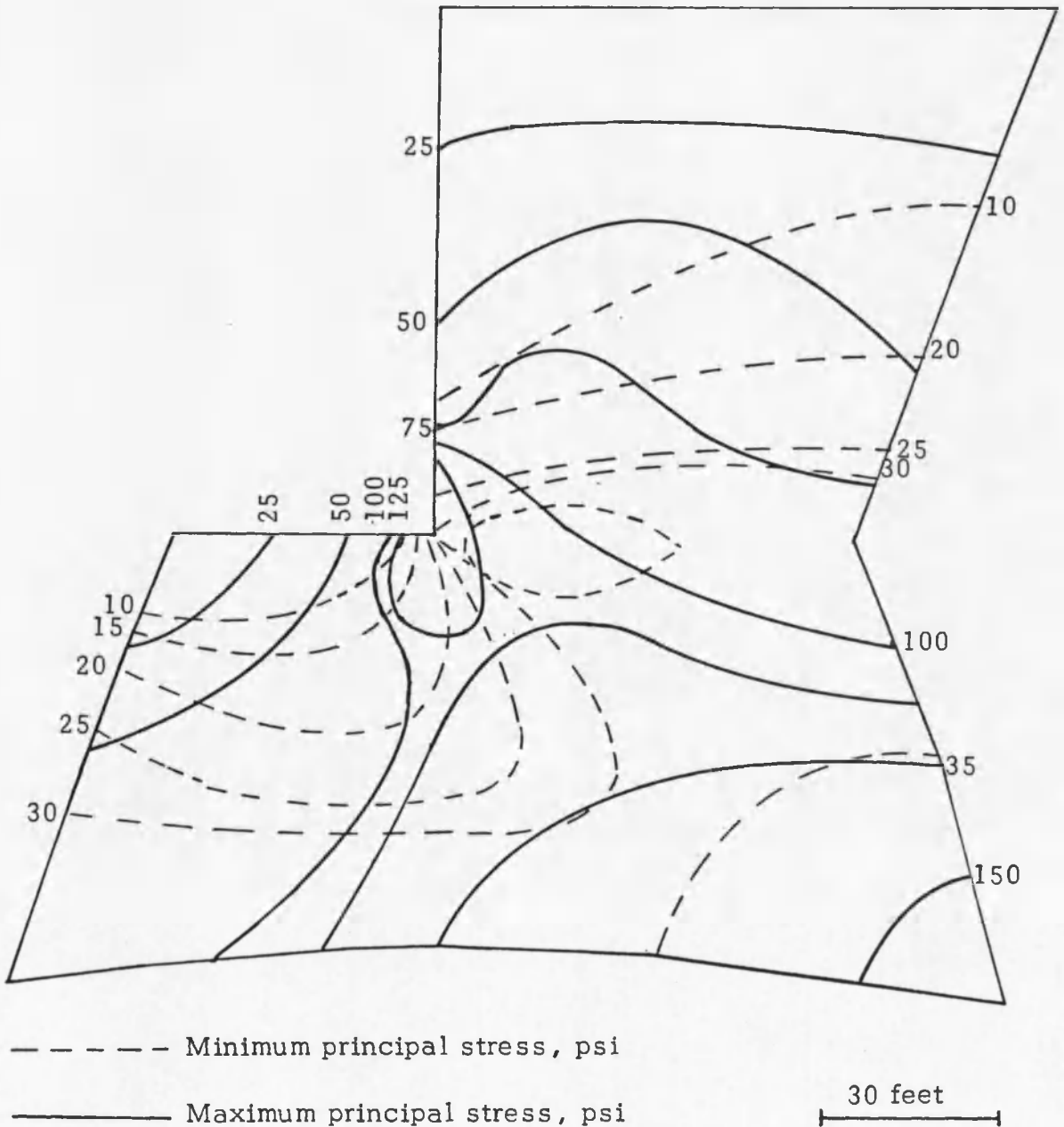


Figure 20. Maximum and minimum principal stresses, section A of rock-wall mesh, unequal horizontal stresses applied

Displacement of nodal points is vertical and a function of the height above the base, as would be expected. The higher the nodal point, the more displacement it assumes (Fig. C-2, Appendix C). An analogy to this would be the effect of weight hanging from a spring. The higher segments assume maximum displacement while the lower ones have minimum displacement. The application of horizontal stress has little effect next to where the pressure is applied; however, the horizontal stress does not seem to affect the direction of displacement of any of the interior points.

## CHAPTER 7

### CONCLUSIONS

The solutions presented in this thesis can be used for many different earth features and engineering problems. Areas that are prone to mud slides could be secured if the physical properties were obtained for the water-saturated soil. The knowledge of the stress field around a notch has its application in tunnel engineering.

The finite element solution for the Hochkönig massif appears to be correct as far as the alignment of the principal stresses and their magnitudes. A. E. Scheidegger (written commun., 1975) reports that the calculated stresses are within 10 to 12 percent of the measured ones. This deviation from the measured results can be attributed to the assumption that each layer is homogeneous and has a single Poisson ratio or to the size chosen for the elements. The smaller the elements, the closer the approximation is to the true principal stress. The direction of the calculated principal stress axes are consistent with those that were measured (Fig. 21).

The Mohr criteria were applied in this study. These failure criteria are not the only ones that could have been used. They use as essential data the principal stresses. Obviously, all calculated results can be used in applying other criteria of failure.

The study of the rock wall determined the concentrations of maximum and minimum principal stresses at the notch itself. There was

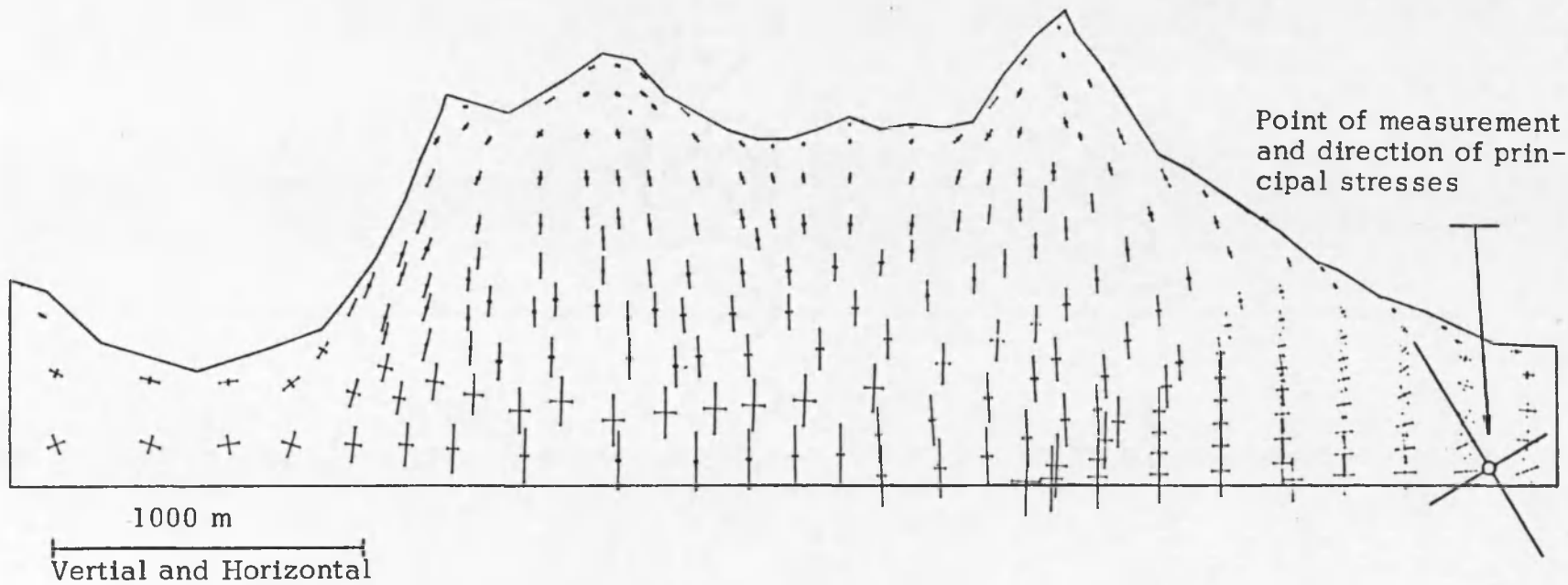


Figure 21. Directions of maximum and minimum principal stresses for Alpine cross section

no appreciable change in the stress field surrounding the notch due to the applications of equal and opposite pressures. Application of the Mohr criteria without consideration of the confining pressure caused the apparent failure away from the notch (Fig. C-3, Appendix C).

## APPENDIX A

### DEFINITION OF TERMS

Doorstopper method—a method described by Leeman (1964) used to determine the stresses in rock by cementing strain gages to a smoothed end of a borehole and measuring the relief brought about by overcoring the gages with an annulus having an outside diameter that is the same as the inside diameter of the original borehole. As the coring is continued past the gage, a strain is recorded that is related to the in situ stresses in the rock.

Endogenic weathering—weathering of a rock mass that is caused by the action of a stress field on it.

Exogenic weathering—weathering occurring in the upper crust due to atmospheric influence or to the influence of ice and water. These factors weaken the cohesion between rock particles and make the rock vulnerable to fluvial agents.

Conjugate joints—two joint sets created by a set of principal stresses where their planes form an angle of 40-60 degrees with the maximum principal stress; consistent with Coulomb-Mohr theory.

Isobar—a line of constant principal stress.

Isochromatic—a curve along which the differences between principal stresses are constant; seen in photoelastic experiments.

Isoclinic—a curve on which the principal axis makes a constant angle to a specified direction; readily observed by photoelastic observations.

Isopach—a curve along which the sum of the principal stresses is constant.

Residual stresses—stresses that exist in the earth's crust due to pre-existing tectonic stresses or the self-equilibrating stress components that remain after the external forces and moments are removed.

Rheology—the study of flowage of materials, particularly plastic flow of solids.

Slip line—a line of equal maximum shearing stress. This orthogonal family of curves bisects the angle between the directions of the principal stresses.

Stress trajectory—a curve having the property that the tangent at every point gives the principal axis of stress.

APPENDIX B

ALPINE SOLUTION

ALPINE PROBLFM.

NUMBER OF NODAL POINTS----- 245  
 NUMBER OF ELEMENTS----- 240  
 NUMBER OF DIFF. MATERIALS--- 4  
 NUMBER OF PRESSURE CARDS---- -0  
 AXIAL ACCELERATION----- .1000E+01  
 ANGULAR VELOCITY----- -0.  
 MAXIMUM NODES DIFFERENCE---- 20  
 REFERENCE TEMPERATURE----- -0.  
 NUMBER OF APPROXIMATIONS---- 1  
 NUMBER OF CUTS----- -0  
 INITIAL RESIDUAL STRESSES--- -0

VALUE OF NPP = -1

VALUE OF NPP = -1

PLANE STRAIN STRUCTURE

MATERIAL NUMBER= 1, NUMBER OF TEMPERATURE CARDS= 1, MASS DENSITY= .2500E-02, MODULUS RATIO= -0.							
TEMPERATURE	E (RZ)	NU (RZ)	E (T)	NU (T)	ALPHA (RZ)	ALPHA (T)	YIELD STRESS
-0.00	.64000E+06	.21000E+00	.64000E+06	.21000E+00	-0.	-0.	-0.
MATERIAL NUMBER= 2, NUMBER OF TEMPERATURE CARDS= 1, MASS DENSITY= .2500E-02, MODULUS RATIO= -0.							
TEMPERATURE	E (RZ)	NU (RZ)	E (T)	NU (T)	ALPHA (RZ)	ALPHA (T)	YIELD STRESS
-0.00	.32000E+06	.21000E+00	.32000E+06	.21000E+00	-0.	-0.	-0.
MATERIAL NUMBER= 3, NUMBER OF TEMPERATURE CARDS= 1, MASS DENSITY= .2500E-02, MODULUS RATIO= -0.							
TEMPERATURE	E (RZ)	NU (RZ)	E (T)	NU (T)	ALPHA (RZ)	ALPHA (T)	YIELD STRESS
-0.00	.11000E+06	.34000E+00	.11000E+06	.34000E+00	-0.	-0.	-0.
MATERIAL NUMBER= 4, NUMBER OF TEMPERATURE CARDS= 1, MASS DENSITY= .2700E-02, MODULUS RATIO= -0.							
TEMPERATURE	E (RZ)	NU (RZ)	E (T)	NU (T)	ALPHA (RZ)	ALPHA (T)	YIELD STRESS
-0.00	.24000E+06	.34000E+00	.24000E+06	.34000E+00	-0.	-0.	-0.

Elem. No.	Element X	Centroid Y	$\sigma_H$	$\sigma_V$	$\tau$	$\sigma_3$	$\sigma_1$	Angle to $\sigma_1$	
1	339000.00	244666.67	-.4518E+01	-.6667E+01	0.	-.2019E-10	-.4518E+01	-.6667E+01	-90.00
2	339500.00	236000.00	-.9665E+01	-.1829E+02	0.	.3723E+01	-.7393E+01	-.1956E+02	-18.86
3	326566.67	234000.00	-.1301E+02	-.1645E+02	0.	-.1450E+02	-.1314E+00	-.2933E+02	-41.62
4	203333.33	229666.67	-.2154E+02	-.1409E+02	0.	.1868E+02	.1244E+01	-.3688E+02	50.64
5	195000.00	233000.00	-.1734E+02	-.8333E+01	0.	.3241E+01	-.7239E+01	-.1834E+02	72.13
6	186666.67	232333.33	-.2352E+02	-.6059E+01	0.	-.9255E+01	-.2066E+01	-.2751E+02	-66.66
7	153333.33	158666.67	-.1953E+02	-.1403E+03	0.	-.9290E+01	-.1882E+02	-.1410E+03	-4.37
8	146000.00	220000.00	-.1909E+02	-.5000E+01	0.	-.3303E-10	-.5000E+01	-.1909E+02	-90.00
9	173333.33	222000.00	-.3723E+02	-.1879E+02	0.	-.1978E+02	-.6190E+01	-.4984E+02	-57.49
10	185000.00	224000.00	-.2489E+02	-.1711E+02	0.	-.5290E+01	-.1444E+02	-.2757E+02	-63.15
11	195000.00	224000.00	-.2229E+02	-.1813E+02	0.	.4048E+01	-.1566E+02	-.2476E+02	58.59
12	203333.33	224000.00	-.2844E+02	-.1989E+02	0.	.1421E+02	-.9315E+01	-.3900E+02	53.38
13	206566.67	220000.00	-.2184E+02	-.2161E+02	0.	.1039E+02	-.1133E+02	-.3212E+02	45.31
14	216566.67	218333.33	-.2894E+02	-.2297E+02	0.	.2399E+02	-.8894E+00	-.4903E+02	47.37
15	270000.00	214333.33	-.3854E+00	-.3333E+01	0.	-.2202E-10	-.3854E+00	-.3333E+01	-90.00
16	290000.00	213666.67	-.1120E+02	-.1667E+01	0.	-.4771E-10	-.1667E+01	-.1120E+02	-90.00
17	316666.67	221000.00	-.2729E+02	-.3995E+02	0.	-.3152E+02	-.1470E+01	-.6577E+02	-39.32
18	325000.00	224000.00	-.2862E+02	-.3647E+02	0.	-.1307E+02	-.1326E+02	-.4384E+02	-29.38
19	340000.00	223000.00	-.1594E+02	-.3353E+02	0.	.6722E+01	-.1367E+02	-.3580E+02	18.70
20	348000.00	227000.00	-.1258E+02	-.2988E+02	0.	.1022E+02	-.7859E+01	-.3471E+02	24.80
21	358000.00	210333.33	-.2404E+02	-.6902E+02	0.	.2308E+02	-.1430E+02	-.7876E+02	22.87
22	344666.67	210333.33	-.1611E+02	-.3277E+02	0.	.6371E+01	-.1395E+02	-.3493E+02	18.70
23	340000.00	214666.67	-.1944E+02	-.4507E+02	0.	.8822E+01	-.1670E+02	-.4782E+02	17.27
24	325000.00	211500.00	-.1917E+02	-.4673E+02	0.	-.1021E+02	-.1489E+02	-.5000E+02	-17.78
25	315000.00	210750.00	-.2689E+02	-.4595E+02	0.	-.1751E+02	-.1649E+02	-.5636E+02	-39.73
26	305000.00	209500.00	-.3464E+02	-.3120E+02	0.	-.2035E+02	-.1250E+02	-.5334E+02	-47.41
27	290000.00	209000.00	-.1382E+02	-.1479E+02	0.	-.5027E+01	-.9259E+01	-.1936E+02	-42.24
28	270000.00	209000.00	-.3901E+01	-.1367E+02	0.	-.9892E+00	-.3703E+01	-.1377E+02	-5.67
29	255000.00	208250.00	-.5512E-01	-.1008E+02	0.	-.1124E+01	.6933E-01	-.1820E+02	-6.32
30	245000.00	207500.00	-.3930E+01	-.7774E+01	0.	.3513E+01	-.1849E+01	-.9860E+01	30.64
31	235000.00	208250.00	-.1713E+02	-.1642E+02	0.	.1215E+02	-.4621E+01	-.2893E+02	45.83
32	220000.00	210250.00	-.2431E+02	-.3127E+02	0.	.1659E+02	-.1883E+02	-.4474E+02	39.08
33	205000.00	211500.00	-.2070E+02	-.3944E+02	0.	.1155E+02	-.1520E+02	-.4494E+02	25.47
34	195000.00	211500.00	-.2102E+02	-.4085E+02	0.	.5091E+01	-.1979E+02	-.4208E+02	13.59
35	185000.00	211500.00	-.2700E+02	-.3872E+02	0.	-.4205E+00	-.2299E+02	-.3873E+02	-1.53
36	170000.00	211500.00	-.3032E+02	-.3460E+02	0.	-.7484E+01	-.2467E+02	-.4024E+02	-37.01
37	153333.33	209333.33	-.2064E+02	-.2785E+02	0.	-.1550E+02	-.8336E+01	-.4015E+02	-38.45
38	146000.00	213666.67	-.2457E+02	-.2552E+02	0.	-.1359E+02	-.1149E+02	-.3869E+02	-43.89
39	136566.67	209333.33	-.1392E+02	-.2491E+02	0.	-.2026E+02	.3524E+01	-.3935E+02	-35.48
40	134500.00	197500.00	-.2029E+02	-.6762E+02	0.	-.3198E+02	-.4173E+01	-.8373E+02	-26.75
41	150000.00	197500.00	-.2263E+02	-.5472E+02	0.	-.1757E+02	-.1488E+02	-.6247E+02	-23.80
42	170000.00	197500.00	-.1998E+02	-.6099E+02	0.	-.5954E+01	-.1914E+02	-.6093E+02	-8.08
43	185000.00	197500.00	-.1672E+02	-.6751E+02	0.	.2576E+01	-.1659E+02	-.6774E+02	2.89
44	195000.00	197500.00	-.1595E+02	-.6868E+02	0.	.6481E+01	-.1517E+02	-.6947E+02	6.91
45	205000.00	197500.00	-.1590E+02	-.6773E+02	0.	.1098E+02	-.1368E+02	-.6995E+02	11.48
46	220000.00	197500.00	-.1678E+02	-.6046E+02	0.	.1589E+02	-.1161E+02	-.6563E+02	18.02
47	235000.00	197500.00	-.1624E+02	-.4886E+02	0.	.1553E+02	-.1003E+02	-.5507E+02	21.80
48	245000.00	197500.00	-.1393E+02	-.4176E+02	0.	.8459E+01	-.1147E+02	-.4412E+02	15.61
49	255000.00	197500.00	-.1385E+02	-.4155E+02	0.	.1286E+01	-.1080E+02	-.4161E+02	2.39
50	270000.00	197500.00	-.1136E+02	-.4481E+02	0.	-.3806E+01	-.1094E+02	-.4523E+02	-6.41

Elem. No.	Element X	Centroid Y	$\sigma_H$	$\sigma_V$	$\tau$	$\sigma_3$	$\sigma_1$	Angle to $\sigma_1$	
51	290000.00	197500.00	-.1569E+02	-.5045E+02	0.	-.1136E+02	-.1230E+02	-.5393E+02	-16.58
52	305000.00	197500.00	-.1559E+02	-.6024E+02	0.	-.1676E+02	-.9999E+01	-.6593E+02	-18.45
53	315000.00	197500.00	-.1330E+02	-.6863E+02	0.	-.1160E+02	-.1097E+02	-.7096E+02	-11.38
54	325000.00	197500.00	-.1053E+02	-.8151E+02	0.	-.2446E+01	-.1044E+02	-.8159E+02	-1.97
55	336000.00	199250.00	-.1844E+02	-.8239E+02	0.	-.3697E+00	-.1844E+02	-.8240E+02	-.33
56	354500.00	206000.00	-.1392E+02	-.5194E+02	0.	.1074E+02	-.1110E+02	-.5476E+02	14.74
57	372500.00	197250.00	-.2537E+02	-.7197E+02	0.	.3340E+02	-.7945E+01	-.8939E+02	27.55
58	395333.33	192333.33	-.1317E+02	-.2114E+02	0.	.1214E+02	-.4379E+01	-.2993E+02	35.91
59	367500.00	186000.00	.4096E+01	-.6037E+02	0.	.2375E+02	.1190E+02	-.6818E+02	18.19
60	348500.00	189500.00	-.7587E+01	-.8138E+02	0.	.4769E+01	-.7240E+01	-.8168E+02	3.68
61	333333.33	190666.67	-.5897E+00	-.1193E+03	0.	-.2632E+01	-.5313E+00	-.1193E+03	-1.27
62	325000.00	187250.00	.5168E+01	-.9893E+02	0.	.2476E+01	.5227E+01	-.9899E+02	1.36
63	315000.00	186000.00	-.1822E+01	-.8873E+02	0.	-.9330E+01	-.8319E+00	-.8972E+02	-6.06
64	305000.00	184000.00	-.9228E+01	-.9291E+02	0.	-.9619E+01	-.8136E+01	-.9400E+02	-6.47
65	290000.00	183000.00	-.1655E+02	-.9023E+02	0.	-.9838E+01	-.1526E+02	-.9152E+02	-7.48
66	270000.00	183000.00	-.1806E+02	-.8669E+02	0.	-.4600E+01	-.1775E+02	-.8699E+02	-3.82
67	255000.00	183000.00	-.1839E+02	-.8669E+02	0.	.2814E+01	-.1827E+02	-.8680E+02	2.36
68	245000.00	184750.00	-.1935E+02	-.8263E+02	0.	.1141E+02	-.1736E+02	-.8463E+02	9.91
69	235000.00	184750.00	-.1831E+02	-.8531E+02	0.	.1277E+02	-.1595E+02	-.8767E+02	10.43
70	220000.00	183000.00	-.1432E+02	-.9478E+02	0.	.1457E+02	-.1177E+02	-.9734E+02	9.95
71	205000.00	183000.00	-.1286E+02	-.9750E+02	0.	.1072E+02	-.1153E+02	-.9883E+02	7.11
72	195000.00	185000.00	-.1239E+02	-.9508E+02	0.	.6209E+01	-.1193E+02	-.9554E+02	4.27
73	190000.00	178666.67	-.8037E+01	-.1092E+03	0.	.4653E+01	-.7824E+01	-.1094E+03	2.63
74	185000.00	185000.00	-.1239E+02	-.9398E+02	0.	.2830E+01	-.1229E+02	-.9408E+02	1.98
75	170000.00	183000.00	-.1196E+02	-.8897E+02	0.	-.2836E+01	-.1185E+02	-.8908E+02	-2.11
76	150000.00	183000.00	-.1557E+02	-.7810E+02	0.	-.1423E+02	-.1248E+02	-.8118E+02	-12.24
77	131500.00	183750.00	-.1677E+02	-.9092E+02	0.	-.3913E+02	.6323E-01	-.1077E+03	-23.27
78	133333.33	175333.33	-.9481E+01	-.8754E+02	0.	-.4442E+02	.1062E+02	-.1076E+03	-24.35
79	150000.00	172250.00	-.6877E+01	-.9720E+02	0.	-.1144E+02	-.5450E+01	-.9863E+02	-7.11
80	170360.00	179000.00	-.3202E+01	-.1172E+03	0.	-.1309E+01	-.3187E+01	-.1172E+03	-.66
81	190000.00	168500.00	-.8157E+01	-.1246E+03	0.	.8973E+00	-.8151E+01	-.1286E+03	.43
82	205000.00	167500.00	-.1084E+02	-.1313E+03	0.	.9990E+01	-.1001E+02	-.1322E+03	4.71
83	217500.00	167250.00	-.1565E+02	-.1327E+03	0.	.9727E+01	-.1484E+02	-.1335E+03	4.72
84	240000.00	174333.33	-.1642E+02	-.9836E+02	0.	.1159E+02	-.1481E+02	-.9997E+02	7.90
85	235000.00	167750.00	-.1900E+02	-.1312E+03	0.	.1021E+02	-.1808E+02	-.1321E+03	5.15
86	250000.00	169250.00	-.2301E+02	-.1310E+03	0.	.5220E+01	-.2276E+02	-.1312E+03	2.76
87	265000.00	169500.00	-.2324E+02	-.1291E+03	0.	-.2473E+01	-.2319E+02	-.1292E+03	-1.34
88	280000.00	171000.00	-.2374E+02	-.1210E+03	0.	-.8487E+01	-.2391E+02	-.1217E+03	-4.95
89	290000.00	174666.67	-.1639E+02	-.1009E+03	0.	-.3644E+01	-.1623E+02	-.1009E+03	-2.47
90	300000.00	181500.00	-.4552E+01	-.1043E+03	0.	.3302E+01	-.4443E+01	-.1044E+03	1.89
91	330000.00	176000.00	-.5750E+01	-.1174E+03	0.	.1079E+00	-.5750E+01	-.1174E+03	.06
92	320000.00	170500.00	-.7654E+01	-.1299E+03	0.	-.1742E+01	-.7629E+01	-.1299E+03	-.82
93	310000.00	165750.00	-.1208E+02	-.1416E+03	0.	-.1987E+01	-.1205E+02	-.1416E+03	-.88
94	295000.00	160500.00	-.1579E+02	-.1448E+03	0.	.1573E+01	-.1577E+02	-.1448E+03	.70
95	271500.00	156500.00	-.2999E+02	-.1641E+03	0.	-.1775E+01	-.2996E+02	-.1642E+03	-.76
96	250000.00	155250.00	-.3142E+02	-.1681E+03	0.	.2300E+01	-.3138E+02	-.1681E+03	.96
97	231750.00	154750.00	-.2958E+02	-.1661E+03	0.	.6638E+01	-.2925E+02	-.1665E+03	2.78
98	215750.00	154250.00	-.2776E+02	-.1625E+03	0.	.8866E+01	-.2718E+02	-.1631E+03	3.75
99	206666.67	156000.00	-.2679E+02	-.1627E+03	0.	.1116E+01	-.2678E+02	-.1627E+03	.47
100	198000.00	153333.33	-.2041E+02	-.1611E+03	0.	.3431E+01	-.2033E+02	-.1612E+03	1.40

Elem. No.	Element X	Centroid Y	$\sigma_H$	$\sigma_V$	$\tau$	$\sigma_3$	$\sigma_1$	Angle to $\sigma_1$	
101	188000.90	157333.33	-.2189E+02	-.1464E+03	0.	.3109E+01	-.2182E+02	-.1464E+03	1.43
102	174666.67	159333.33	-.2080E+02	-.1523E+03	0.	-.3959E+01	-.2068E+02	-.1525E+03	-1.72
103	146666.67	165666.67	-.1449E+02	-.1075E+03	0.	-.8179E+01	-.1377E+02	-.1082E+03	-4.99
104	133333.33	163666.67	-.2013E+02	-.1090E+03	0.	-.3203E+02	-.9781E+01	-.1193E+03	-17.90
105	125333.33	167333.33	-.2162E+02	-.1013E+03	0.	-.3125E+02	-.1081E+02	-.1121E+03	-19.06
106	125333.33	173666.67	-.2467E+02	-.1127E+03	0.	-.3384E+02	-.1317E+02	-.1242E+03	-18.77
107	114666.67	163666.67	-.2912E+02	-.1112E+03	0.	-.4057E+02	-.1245E+02	-.1279E+03	-22.34
108	109333.33	156666.67	-.1865E+02	-.7178E+02	0.	-.3346E+02	-.2494E+01	-.8794E+02	-25.78
109	120000.00	153333.33	-.2110E+02	-.1230E+03	0.	-.3229E+02	-.1173E+02	-.1324E+03	-16.19
110	133333.33	156666.67	-.2348E+02	-.1216E+03	0.	-.3405E+02	-.1281E+02	-.1323E+03	-17.39
111	146666.67	153333.33	-.1106E+02	-.1180E+03	0.	-.2585E+01	-.9998E+01	-.1181E+03	-1.37
112	168000.00	155333.33	-.1492E+02	-.1390E+03	0.	.5178E+00	-.1492E+02	-.1391E+03	.24
113	120000.00	148333.33	-.1402E+02	-.9636E+02	0.	-.2238E+02	-.8331E+01	-.1021E+03	-14.27
114	133333.33	144666.67	-.1706E+02	-.1493E+03	0.	-.3456E+02	-.8548E+01	-.1574E+03	-13.83
115	147500.00	143500.00	-.1668E+02	-.1602E+03	0.	-.8251E+01	-.1621E+02	-.1607E+03	-3.28
116	156666.67	139333.33	-.2690E+02	-.1747E+03	0.	-.6791E+01	-.2659E+02	-.1750E+03	-2.62
117	173500.00	140750.00	-.2491E+02	-.1856E+03	0.	-.3691E+01	-.2483E+02	-.1857E+03	-1.31
118	198500.00	140375.00	-.2703E+02	-.1954E+03	0.	-.1205E+01	-.2702E+02	-.1954E+03	-.41
119	213333.33	137833.33	-.2108E+02	-.1934E+03	0.	.4891E+01	-.2094E+02	-.1935E+03	1.62
120	220750.00	141000.00	-.2695E+02	-.1941E+03	0.	.7626E+01	-.2660E+02	-.1945E+03	2.61
121	236750.00	141500.00	-.3306E+02	-.2022E+03	0.	.3887E+01	-.3292E+02	-.2023E+03	1.32
122	260000.00	143500.00	-.3571E+02	-.1991E+03	0.	-.4866E+00	-.3571E+02	-.1991E+03	-.17
123	282000.00	146666.67	-.3478E+02	-.1896E+03	0.	-.1357E+01	-.3477E+02	-.1896E+03	-.50
124	360000.00	175000.00	-.1060E+02	-.1115E+03	0.	.9537E+01	-.9703E+01	-.1124E+03	5.35
125	350000.00	165500.00	-.1557E+02	-.1292E+03	0.	.4602E+01	-.1539E+02	-.1294E+03	2.31
126	340000.00	157500.00	-.3088E+02	-.1535E+03	0.	-.6568E+00	-.3087E+02	-.1535E+03	-.31
127	330000.00	151250.00	-.4634E+02	-.1750E+03	0.	-.4434E+01	-.4619E+02	-.1751E+03	-1.97
128	317500.00	146000.00	-.5680E+02	-.1944E+03	0.	-.7607E+01	-.6635E+02	-.1949E+03	-3.40
129	300000.00	138750.00	-.6815E+02	-.1954E+03	0.	-.3064E+01	-.6808E+02	-.1955E+03	-1.38
130	277500.00	131000.00	-.9380E+02	-.2261E+03	0.	-.6045E+01	-.9352E+02	-.2264E+03	-2.61
131	255000.00	127000.00	-.1075E+03	-.2421E+03	0.	-.6725E+01	-.1072E+03	-.2424E+03	-2.85
132	238500.00	125500.00	-.1104E+03	-.2455E+03	0.	-.5203E+01	-.1102E+03	-.2457E+03	-2.20
133	226000.00	124375.00	-.1071E+03	-.2413E+03	0.	-.3207E+01	-.1070E+03	-.2414E+03	-1.37
134	219000.00	123125.00	-.1063E+03	-.2391E+03	0.	-.1533E+01	-.1063E+03	-.2392E+03	-.66
135	193333.33	120666.67	-.1042E+03	-.2411E+03	0.	.6480E-02	-.1042E+03	-.2411E+03	.00
136	176666.67	126666.67	-.1377E+03	-.2285E+03	0.	-.3633E+01	-.1076E+03	-.2286E+03	-1.72
137	163333.33	123666.67	-.9869E+02	-.2153E+03	0.	-.4537E+00	-.9869E+02	-.2153E+03	-.22
138	148500.00	128750.00	-.9204E+02	-.1942E+03	0.	-.5427E+01	-.9175E+02	-.1945E+03	-3.03
139	136000.00	132750.00	-.8327E+02	-.1697E+03	0.	-.1022E+02	-.9208E+02	-.1709E+03	-6.66
140	120000.00	137250.00	-.7093E+02	-.1279E+03	0.	-.1435E+02	-.6752E+02	-.1313E+03	-13.38
141	100000.00	142875.00	-.5494E+02	-.7490E+02	0.	-.2173E+02	-.4102E+02	-.8883E+02	-32.67
142	4000.00	163833.33	-.4975E+01	-.1425E+01	0.	.1053E+01	-.1137E+01	-.5264E+01	74.66
143	10500.00	154000.00	-.3152E+02	-.1825E+02	0.	.1105E+02	-.1206E+02	-.3777E+02	60.50
144	15000.00	135500.00	-.6055E+02	-.4341E+02	0.	.1134E+02	-.3777E+02	-.6619E+02	63.54
145	45000.00	133250.00	-.9006E+02	-.3225E+02	0.	.1661E+02	-.2781E+02	-.9449E+02	75.06
146	70900.00	132625.00	-.8819E+02	-.2662E+02	0.	-.8114E+01	-.2557E+02	-.8924E+02	-82.62
147	90000.00	132125.00	-.7401E+02	-.6215E+02	0.	-.2764E+02	-.3981E+02	-.9635E+02	-51.05
148	110000.00	129250.00	-.6977E+02	-.1275E+03	0.	-.1942E+02	-.6385E+02	-.1334E+03	-16.97
149	124666.67	127666.67	-.5842E+02	-.1496E+03	0.	-.1576E+02	-.5577E+02	-.1523E+03	-9.53
150	15000.00	113000.00	-.9734E+02	-.9290E+02	0.	.2612E+01	-.8631E+02	-.9393E+02	21.61